

# Exploring Geoscience with cold atom Quantum Gravimeter

*A dissertation submitted in partial fulfillment of the requirement for  
the degree of*  
**Master of Technology**  
in  
**Applied Optics**

*submitted by*  
Jyoti Bej  
2021PHA2469  
*under the guidance of*  
Prof. Bodhaditya Santra



Department of Physics  
Indian Institute of Technology Delhi  
May 10, 2023


# Declaration

I hereby certify that the work embodied in this dissertation entitled "Exploring Geoscience with cold atom Quantum Gravimeter" by **Ms.Jyoti Bej** (2021PHA2469), in the partial fulfillment of the requirement for the award of the degree of 2 years M. Tech program in Applied Optics submitted to the Department of Physics, Indian Institute of Technology Delhi, India, is an authentic record of my work carried out under the supervision of Asst. Prof. Bodhaditya Santra. I have followed ethics to the best of my abilities. I have completed all pre-submission requirements as per the institute's rules. The matter presented in the dissertation has not been submitted by me to any other University/Institute for the award of any other degree or diploma.

Jyoti Bej  
Jyoti Bej  
2021PHA2469 11/05/23

## THESIS CERTIFICATE

This is to certify that the thesis entitled "**Exploring Geoscience with cold atom Quantum Gravimeter**" submitted by Ms. **Jyoti Bej** to the Indian Institute of Technology, Delhi for the award of the degree of Master of Technology is a bonafide record of research work carried out by her under my supervision. She has fulfilled the mandatory requirements for the submission of this dissertation work. In my opinion, this work is fully adequate, in scope and quality, as a dissertation for the degree of Master of Technology in Applied Optics. The contents of this thesis, in full or in parts, have not been submitted to any other Institute/University/Organisation for the award of any degree /diploma.

Sign:  11/05/2023  
**Prof. Bodhaditya Santra**  
Associate Professor  
Department of Physics  
Indian Institute of Technology Delhi  
New Delhi, India

Place: Delhi  
Date: May 2023

Dedicated to my parents

## ACKNOWLEDGEMENTS

First of all, I am very grateful for all the people who gave me advice and assistance with my MTech dissertation project. I never would have been successfully completing my dissertation without their help. It was a great journey

I am heartily thankful to my supervisor **Dr.Bodhaditya Santra** for all of his assistance and words of wisdom throughout the project. I could not complete my work without his contributions. Always behaves like a friend. I learned more new things from his lab. I appreciate his constant advice, tolerance, and insightful criticism, all of which have surely improved the caliber of my research.

I am also extremely grateful to my teaching assistant, **Apoorav Singh Deo** for his persistent assistance and guidance.

They have always believed in me, and their passion, support, and encouragement have been really beneficial. During the dissertation study, his timely encouragement was a huge assistance to me. I want to express my gratitude to my friends for their support and encouragement. They made it possible since we couldn't have done it without them. I dedicate this thesis to my parents and siblings for their unwavering love, immeasurable support, and confidence in my skills.

I want to thank you again to all for your amazing contributions.

Sincerely,  
Jyoti

## ABSTRACT

This study uses a mobile cold atom quantum gravimeter that is established on atom interferometers to find the sources of local gravity anomalies caused by underground geological features. Sub-surface modeling is frequently utilized in domains like civil engineering and mineral exploration, among others. Mapping the subsurface reveals that the object is buried beneath the ground without affecting the test region. Therefore, without altering their chemical or physical signature, such approaches can explore objects that are below the surface. It is possible to see the subsurface of a gravimeter quite precisely. However, a gravity ( $g_z$ ) component alone is insufficient. To more accurately explain subsurface anomalies, the gravity gradient tensor offers a solid foundation. Therefore, utilizing  $g_z$  to obtain the tensor components of gravity can enable us to use the gravity gradient tensor (GGT)-based approach.

# Contents

<b>Declaration</b>	<b>i</b>
<b>Thesis certificate</b>	<b>ii</b>
<b>ACKNOWLEDGEMENTS</b>	<b>iv</b>
<b>ABSTRACT</b>	<b>v</b>
<b>List of Plots</b>	<b>viii</b>
<b>List of Tables</b>	<b>ix</b>
<b>List of Abbreviation</b>	<b>x</b>
<b>1 Introduction and Motivation</b>	<b>1</b>
1.1 An Overview of Gravity . . . . .	1
1.1.1 Earth's gravity and its variations . . . . .	2
1.1.2 Units of gravity . . . . .	2
1.2 Gravity and Gravimetry . . . . .	2
1.2.1 <b>Gravitational Potential</b> . . . . .	3
1.2.2 Gravity Anomaly . . . . .	3
1.2.3 Gravity Gradient Tensor(GGT) . . . . .	4
1.3 Gravimeter . . . . .	7
1.3.1 Relative gravimeter . . . . .	7
1.3.1.1 Mechanical spring-type gravimeters . . . . .	7
1.3.1.2 Superconducting gravimeters . . . . .	8
1.3.2 Absolute Gravimeter . . . . .	9
1.3.3 Atom interferometric-based gravimeters . . . . .	11
1.3.3.1 Working Principle . . . . .	11
1.3.3.2 The Gravimetric Atom Interferometer . . . . .	13
1.4 Applications . . . . .	13
1.5 Use Atom Interferometry(AI) principle . . . . .	14
1.6 Layout of the Thesis . . . . .	14

<b>2</b>	<b>Background Theory</b>	<b>16</b>
2.1	Cold Atoms	16
2.1.1	Optical Molasses and MOT	17
2.2	Raman transition with photon	19
2.2.1	Atom in three-level system	21
2.2.2	Rabi Oscillation	22
2.2.3	Mach-Zehnder Atom interferometry - 3 pulse schemes	24
2.2.4	Phase shift for a constant acceleration	25
2.3	summary	25
<b>3</b>	<b>Towards an efficient Model</b>	<b>26</b>
3.1	Work flow	26
3.2	Forward Model	26
3.2.1	Right rectangular prisms model	27
3.2.2	Drawbacks	29
3.3	The Fourier Model	29
3.3.1	Gravity Gradient Tensor Estimation	30
3.4	Inverse Model	31
3.5	Summary	32
<b>4</b>	<b>Result and Discussion</b>	<b>33</b>
4.1	Forward Model Calculation	33
4.2	Compute Horizontal gravity anomaly elements using the Fourier transform technique	34
4.3	Nine gravity gradient tensor components demonstrate using the Fourier model	35
4.4	Expected Mass and location of the anomaly	37
<b>5</b>	<b>Conclusion and Outlook</b>	<b>39</b>
<b>A</b>		<b>41</b>
A.1	Estimation of Theoretical Mass	41



# List of plots

1.1	Schematic diagram of gravity gradient tensor components . . . . .	4
1.2	Spring type gravimeter . . . . .	8
1.3	Principle of Superconducting gravimeter . . . . .	9
1.4	Absolute Gravimeter . . . . .	10
1.5	Sequence of three laser pulse . . . . .	12
1.6	Schematic of atom interferometry principle: . . . . .	12
2.1	Optical Molasses effect . . . . .	17
2.2	MOT . . . . .	18
2.3	Schematic of Stimulated Raman transition . . . . .	19
2.4	Rabi oscillations . . . . .	23
3.1	Work Flow . . . . .	26
3.2	The right rectangular prism . . . . .	28
4.1	Layout of the scheme . . . . .	33
4.2	$g_z$ . . . . .	34
4.3	$g_x g_y$ . . . . .	34
4.4	$T_{xx} T_{xy}$ . . . . .	35
4.5	$T_{xz} T_{yx}$ . . . . .	35
4.6	$T_{yy} T_{yz}$ . . . . .	36
4.7	$T_{zx} T_{zy}$ . . . . .	36
4.8	$T_{zz}$ . . . . .	37
4.9	Mass Distribution . . . . .	38
4.10	Estimated mass of the object for different densities . . . . .	38

# List of Tables

1.1	Gravity measurement unit in <b>SI</b> and <b>CGS</b> system . . . . .	3
1.2	Predicted values of variations gravitational acceleration in the Earth's surface due to various kinds of sources . . . . .	6
1.3	Compared retail relative gravimeters to their stated specifications . . . . .	9
1.4	Comparison of the absolute gravimeters' with listed parameters in the industrial market . . . . .	11
4.1	Variation of mass with density . . . . .	37

# List of Abbreviation

<b>GGT</b>	Gravity Gradient Tensor
<b>THZ</b>	Total Horizontal Gradient
<b>AI</b>	Atom Interferometry
<b>MOT</b>	Magneto Optical Trap
<b>AG</b>	Absolute gravimeter
<b>MZI</b>	Mach- Zehnder interferometer

# Chapter 1

## Introduction and Motivation

### 1.1 An Overview of Gravity

**Gravity** is a naturally arising marvel that keeps us on the surface of the earth and our circumstances entangled around it. In our four fundamental interactions, the gravitational interaction is  $10^{29}$  to  $10^{28}$  times less than the electromagnetic, weak, and strong interactions. But it has a significant nature from the subatomic particles to macroscopic range masses such as in the field of cosmology. We are familiar with this force in our everyday life. From the earliest times, Scientists are busy rummaging to explore the principles of gravity. In the history of Science, one of the greatest anecdotes Sir **Isaac Newton** gives an idea on the theory of gravity from the story of an apple falling on the earth's surface. The famous philosopher Galileo's free-falling experiment and his determination that "all matter accelerates at the identical ". Sir Isaac Newton provided the first thorough mathematical exposition in his notable creation in 1687 "Philosophiae Naturalis Principia Mathematica" named universal gravitational law. **Newtonian gravitational law** demonstrated that attracting force( $F_g$ ) between two any objects. This force is directly proportionate to the masses of the entities ( $m_1, m_2$ ) and indirectly varies with the square of the distance ( $r^2$ ) between the center of masses. The mathematical form of this law,

$$F_g = G \left( \frac{m_1 m_2}{r^2} \right) \quad (1.1)$$

Where  $G$  is called a universal constant. This hypothesis addresses the tides as well as the actions of the planets approximately the sun. A century afterward, Using a torsion balance the famous scientist Henry Cavendish first experimentally obtained the gravity between two test objects in his laboratory. The earth's density was calculated from this torsion balance measurement. Nevertheless, the fundamental concept of gravity was still mysterious. Within the first ten years of the 20th century, the greatest physicist Albert Einstein published his General Theory of Relativity (**GTR**) proposes that gravity is caused by the curvature of space-time, the fabric of the galaxy. Using his hypothesis, which was successfully defined in precisely signifying Mercury's trajectory, gravitational redshift, the presence of black holes, gravity-related time lags, and gravitational echoes. The new **LIGO** experiment discovered a gravitational wave indication in September 2015. This appeared to be the direct result of two black holes colliding [1]. It paves a new pioneered

in the study of gravity. In the research field, from the past to now equation(1.1) involves determining the fundamental of physics like the precise measurement of gravitational constant( $G$ ) [2], gravitational acceleration( $\vec{g}$ ), the famous inverse square law[3], and the weak equivalence principle [4].

Aspects from these four fundamental laws of physics gravitational law are needed to develop the gravitational force( $F_g$ ) and acceleration due to gravity( $a_g$ ) which acts on the masses of the body. Over the past few years, different kinds of experimental tools have been invented for researching those. Among them, One of the newest technologies Atom interferometers is sensitive to measure the accelerations. Here, describes the new technique for precise measurement of gravity using a Quantum gravimeter based on the atom interferometry principle.

### 1.1.1 Earth's gravity and its variations

A free-fall mass of the object is accelerated to the exterior of the globe due to gravity. From the equation (1.1) Newton's famous law of gravitation, the gravitational aberration due to any mass of the body is

$$g = G \left( \frac{m_e}{R^2} \right) \quad (1.2)$$

Where  $m_e$  and  $R$  represent the earth's mass and radius respectively. So Only uniform or radially categorized spherical body's gravity is calculated using equation (1.4).

The acceleration of gravity affects everything that exists on Earth. Because of the size, shape, and rotation of the Earth, the local gravity involves spatial variability. Variable temporal and spatial effects change the acceleration of gravity. The tidal effect, mass redistribution, polar motion, etc due to these kinds of effects are responsible for changes in the gravity on earth's surface.

### 1.1.2 Units of gravity

Generally, gravity is measured using two systems: The International system (**SI**) and Centimetre-Gram-Seconds (**CGS**) unit system. The name of this unit system is different for different field applications. In the geophysics field, the recommended unit is **GAL** in honor of Galileo. When compared to the Earth's terrestrial variations in gravity, 1 Gal is a significant amount. Another unit, the unit of gravity (**g.u.**), is also utilized for gravity dimensions in various fields, such as the petroleum industry.

Table 1.1 shows the relation between the corresponding units of typical parameters used to measure gravity in the required system. Here, In this thesis, we work on **mGal** and eotvos(**E**) units. Eotvos is the unit of gravity gradient tensor.

## 1.2 Gravity and Gravimetry

The acceleration of gravity which changes from place to place depends on the period. its significance in a wide range of physical sciences, including metrology, geophysics, and

Table 1.1: Gravity measurement unit in **SI** and **CGS** system

Parameters	CGS	SI	In use
Gravitational Force	$10^5 \text{ dynes} (gm \text{ cm} / s^2)$	newtones( <b>N</b> ) $1kg \text{ m} / s^2$	...
Gravitational acceleration	$1Gal$	$10^{-2} m / s^2$	$10^4 \text{ g.u}$
	$1mGal$	$10^{-5} m / s^2$	$10 \text{ g.u}$
	$1\mu Gal$	$10^{-8} m / s^2$	$10^{-2} \text{ g.u}$
Gravity gradient tensor	$10^{-9} Gal / cm$	$10^{-9} / s^2$	1 Eotvots(E)

geodesy. In the Geoscience field, Gravimetry is a well-established technique for determining subsurface mass distribution. Since the whole shape of the Earth, its changes of potential and change of gravity provides valuable messages for defining the geological shape of economic significance. In the geophysical site, The gravity gradient way is one of the most important phenomena that has been effectively used for tracking out remote occurrences of target bodies and to define geological sampling with grown of the resolution. If  $\phi$  defines the potential of gravity,  $g_i$  is the spatial change of potential, and  $\mathcal{G}_{ij}$  presents the spatial variation of gravity then the relation between those are shown in 1.3

$$\begin{array}{c} \nearrow \\ \phi \rightarrow \\ \searrow \end{array} \begin{array}{c} |g_x| \\ |g_y| \\ |g_z| \end{array} \rightarrow \begin{array}{c} | \mathcal{G}_{xx} \quad \mathcal{G}_{xy} \quad \mathcal{G}_{xz} | \\ | \mathcal{G}_{yx} \quad \mathcal{G}_{yy} \quad \mathcal{G}_{yz} | \\ | \mathcal{G}_{zx} \quad \mathcal{G}_{zy} \quad \mathcal{G}_{zz} | \end{array} \quad (1.3)$$

### 1.2.1 Gravitational Potential

At the location, the gravitational potential is measured as gravitational potential energy at that location per unit mass. If Mathematically describes at a field,

$$\phi(x) = \int_{\infty}^x \frac{GM}{x^2} dx \quad (1.4)$$

### 1.2.2 Gravity Anomaly

Generally, the gravity anomaly is the schism between the accomplished acceleration of a free-falling body near the surface of a planet and the corresponding value predicted by a theoretical model of the planet's gravitational field. The unit of gravity anomaly in the **S.I** system is  $m/s^2$  and C.G.S system **Gal** [ $cm/s^2$ ]. Usually, **Gal** unit is used for measuring the gravity anomaly.

Mathematically define the gravity anomaly, as the derivative of gravitational potential with respect to the location.

$$\vec{g} = \frac{\partial \phi}{\partial \vec{r}} \quad (1.5)$$

### 1.2.3 Gravity Gradient Tensor(GGT)

Gravity Gradient Tensor(GGT) tensors defined the rate of change of the spatial coordinate of the vector segments of gravity in all three orders. The eotvos (E) is the unit of this quantity. The gravity gradient tensor is a symmetric, traceless matrix. Mathematically it represents the rate of changes in gravitational acceleration with respect to the position in three dimensions. The fundamental gravity gradient tensor is important in gravity field modeling and analysis. It has numerous significance in various areas, including geodesy, geophysics space missions, and satellite navigation. The gravity gradient tensor is used in gravity field modeling, which uses gravitational data to determine the mass distribution inside the earth's surface.

$$G_{ij} = \frac{\partial g_i}{\partial j} \quad (1.6)$$

Where  $i, j = x, y, z$

$$G = \begin{bmatrix} G_{xx} & G_{xy} & G_{xz} \\ G_{yx} & G_{yy} & G_{yz} \\ G_{zx} & G_{zy} & G_{zz} \end{bmatrix} \quad (1.7)$$

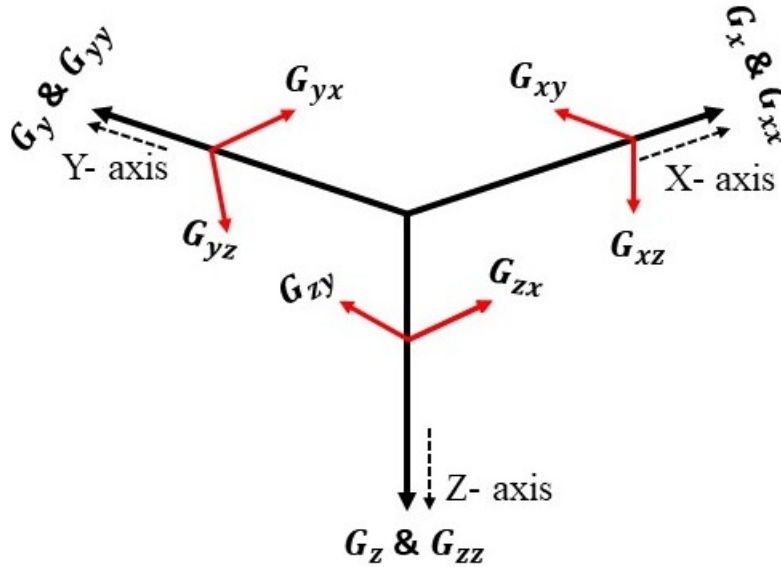


Figure 1.1: Schematic diagram of gravity gradient tensor components

- It is a  $3 \times 3$  real trace less symmetric matrix.
- Since the gravitational potential is a scalar quantity, it's gratify the Laplace equation  $\nabla^2 \phi = 0$  then the aggregate of the diagonal components is zero which means the trace of the matrix is zero.  $G_{xx} + G_{yy} + G_{zz} = 0$

- Since it is a symmetric tensor then it has six independent components [ $G_{ij} = G_{ji}$ ] when  $i \neq j$

$$G_{xy} = G_{yx}$$

$$G_{xz} = G_{zx}$$

$$G_{yz} = G_{zy}$$

- **Significance**

Figure 1.1 exhibits the Schematic description of the gravity gradient tensor. Typical gravity information demonstrates the potency of the earth's gravity domain but it is slightly sensitive to object boundaries and missing the directional data. Gravity gradients directly recover acute signals across the borders of structures and are strongly connected to the causative entities like rims, intersections, and centers of mass, producing complex layouts of the anomalies. The six gravity gradient details diagonal (or axial) elements or the rotational segments from the whole tensor form are a workable implement for prescribing the structure of the body. Gravity gradients substantially resemble the sides, corners, and center of mass of the etiological bodies and retrieve powerful signals over the periphery of structures.

- **$G_{zz}$**  — It always delivers the most powerful signal, but it also contains a significant amount of geological and acquisition disturbance. Typically exhibits relatively invariant behavior, which means that as the vertical signal, it shows the least observation direction reliance and is numerous reliably analyzed as a "stand-alone" tensor element. The  $G_{zz}$  displays an easier-to-interpret, clearer image of the basement when there are no near-surface geology influences or substantial structural changes. In actuality, the  $G_{zz}$  can frequently be significantly contaminated by shallow geology or residual terrain effects, making low-pass filtering necessary (although this has risks).
- **$G_{yz}$ ,  $G_{xz}$**  — These two tensor elements are the horizontal gradients of gravity with respect to the vertical axis. These elements have a similar nature to the X and Y derivatives of a typical vertical measurement of gravity or magnetic field. They measure the edges of bodies at depth. It is common to combine them to create a measurement known as the Total Horizontal Gradient (**THG**), the mathematically defined Pythagorean measure of the strongest horizontal gradient signal is,

$$THG = \sqrt{(G_{xz}^2 + G_{yz}^2)} \quad (1.8)$$

This can also be referred to as a 2D analytical signal. In general, they can be the second-greatest signal measure after  $G_{zz}$ , although which one conveyed the strongest signal may depend on the geology's orientation to the plane. The **THG** is invariant about the z-axis, making it a preferred interpretative tool for edge mapping and worming (multi-scale edge detection) because this value remains identical no matter how it is measured.



- $G_{xx}$ ,  $G_{yy}$  — These components refer to horizontal gravity gradients in the cardinal directions. Depending on how they are measured, they may differ in signal strength, and this may also significantly alter their anomaly patterns. The magnitude of the aggregate of these effects equals that of the  $G_{zz}$  (Laplace Equation), making it also invariant, but the strength of each component need not be equal. Normally, until they are transformed into an Invariant form, these wouldn't be used for qualitative interpretation.
- $G_{xy}$  — Among the whole gravity gradient tensor components this signal is always the weakest because it has the lowest coupling with subsurface bodies. Although it maps the corners of a vertical body with an opposing anomaly pattern and typically carries an NW-SE/NE-SW fabric on its anomaly pattern. It is extremely rotation-dependent and geometrically sensitive.

If the potential field features of a tensor hold (Laplace Equation), it is mathematically conceivable to use Fourier Transformations to convert any one component into any of the other five independent components. In contrast, direct measurement, doing so results in the introduction of noise and a loss of signal strength.

The below section here describes a tabular form of the magnitude of variation of gravitational acceleration due to different kinds of sources [5],[6] in **mGal** unit.

Table 1.2: Predicted values of variations gravitational acceleration in the Earth's surface due to various kinds of sources

Source	Magnitude of variations in gravity anomaly(mGal)
Earth	$98 \times 10^4$
Latitudinal Deviation	$5 \times 10^3$
Mountains and ocean ridges	$2 \times 10^2$
aberrations in minerals	$10^2$
Elevation by 1m	$3 \times 10^{-1}$
Solid earth tides	$\pm 15 \times 10^{-3}$
volcanism and earthquakes	$2 \times 10^{-1}$
Lunar/Sun Tides	$10^{-1}$
level of groundwater	$\pm 1 \times 10^{-2}$
post-glacial recovery	$10^{-2}$
Polar spin	$8 \times 10^{-3}$
Polar ice transformation	$5 \times 10^{-3}$
atmospheric pressure	0.003-0.02 (0.0003/hPa <sup>1</sup> )
1m away from the person	$5 \times 10^{-4}$

---

<sup>1</sup>hPa=Hectopascal, unit of pressure

## 1.3 Gravimeter

For gravity studies, highly accurate gravimeters are very important. Our understanding of the gravitational field has been affected by the progress of the gravimeter. Typically, there are two fundamental types of gravimeters: Relative and Absolute gravimeters.

Absolute gravimeters measure gravitational acceleration directly in standard units of length and time ( $m/s^2$ ). Relative gravimeters can only detect variations in gravity. Relative gravimeters are often more sensitive than absolute gravimeters and are simpler to construct in a compact form. Relative gravimeters must be calibrated with a base station, though, in order to uniformly estimate distances in various places. Relative gravimeters also need regular calibration because of the instrument drift. Simple pendulums and torsion balances were initially used for determining the Earth's gravity. The pendulum is the most immature absolute gravimeter, however, it is challenging to obtain accuracy greater than mGal. Because of its considerable sensitivity to ground irregularities, torque balances can only be utilized on very flat terrain. These instruments have been replaced by other instruments during the 20th century since they also required hours of observation [7]. Here describes some of the gravimeters.

### 1.3.1 Relative gravimeter

The relative gravimeter is just a keen scale that measures changes in  $g$ . Maintaining the examination mass balanced in the gravitational field is the essential idea, and the fluctuations of  $g$  are determined by measuring the counter-reaction significance required to maintain the mass in its equilibrium position. These instruments require an absolute gravimeter to calibrate the scaling factor. Spring-type relative gravimeters are the most common. which means that the force of gravity on a mass is counterbalanced by the force that restores a spring. An example of this type of gravimeter, like Mechanical spring-type gravimeters, Superconducting gravimeters, LA-COSTE ROMBERG gravimeters, etc.

#### 1.3.1.1 Mechanical spring-type gravimeters

The fundamental component of mechanical spring-type gravimeters is a test mass ( $m$ ) that is fixed to a spring. The primary length of this spring is  $l_0$ . Due to **Hook's law**, variations in gravity and the force of gravitational strength acting on the mass as a result of those variations lead to different spring elongations,

$$mg = k(l - l_0) \quad (1.9)$$

where  $k$  is the spring constant, and  $l$  is the length of the spring after attaching the mass. As a result, variations in the spring's elongation are proportional to variations in gravity. Sometimes it is called the zero-length-based spring gravimeter. From Figure 1.3 a hinged cantilever supports the mass, and the torques produced by gravity and the spring force

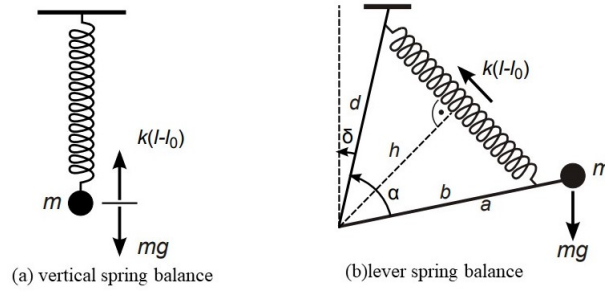


Figure 1.2: Schematic of Spring type based gravimeter[8]

are balanced.

$$mga \sin(\alpha + \delta) = kbd \frac{(l - l_0)}{l} \sin \alpha \quad (1.10)$$

The principle of this kind of gravimeter, For a zero-length spring and  $\alpha + \delta = 0$

$$mga = kbd \sin \alpha \quad (1.11)$$

When  $\alpha = 90^\circ$  the sensitivity is maximum. Today's gravimeters, which operate on a similar principle and are outfitted with position read-out systems with sub-micron resolution, may achieve precisions of at least  $100nm/s^2$ . Due to changes in the spring constant and spring length brought on by aging and environmental factors, mechanical spring-type gravimeters' accuracy is limited. By adopting unique, temperature- and pressure-stabilized housings, these are reduced.

### 1.3.1.2 Superconducting gravimeters

Major problems with the aforementioned spring-type gravimeters include elastic fluctuation of the spring, thermal interference generated by the spring, and the loss of mass from the experimental mass, all of which call for periodic calibration. A recent spring-style gravimeter with little substance is the superconducting gravimeter. The experimental mass, a metallic orb formed of superconducting metal or covered with a coating of it, is lifted by a magnetic domain produced by current drifting in a super-conducting coil that has been refrigerated to 4K.

Mainly Superconducting gravimeters based on magnetic fields. Magnetic fields lift a sphere-shaped specimen of mass in a superconducting gravimeter (SG), which replaces the mechanical spring with magnetic fields. Their superconductive coils permanently maintain an initial current that is set to account for the gravitational force when they are operated at helium temperature. This principle enables the device to attain extremely low and nearly linear drift rates[9]. At the reference position, the test mass must be evenly distributed, changes in current are therefore proportional to changes in gravitational or inertial forces[10]. One of the best sensitivities and long-term stability is achieved by the **iGrav** superconducting gravimeter from GWR devices [11]. Because of this, the **iGrav** is frequently utilized to evaluate and validate other gravimeters. The disadvantages of this kind of gravimeter are it is difficult to in transportation, bulk, and time-consuming setup at new locations.

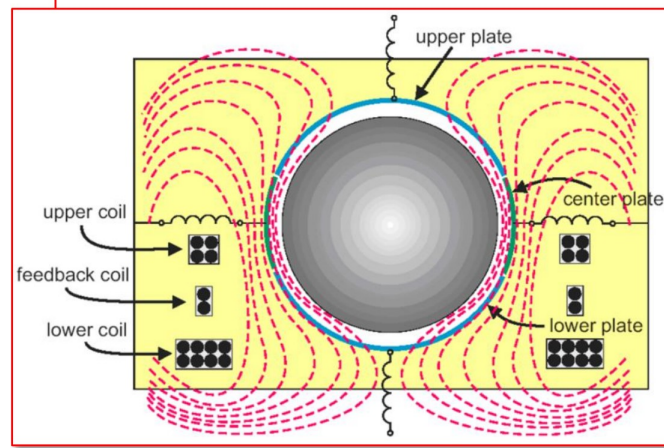


Figure 1.3: Principle of Superconducting gravimeter [11]

Recently, Gravimeters are becoming more compact because of the use of innovative technology in lab prototype systems. A microelectromechanical system (**MEMS**)-based relative gravimeter is one of them. The stability can measure the Earth's tide, and the reported sensitivity is  $40\mu\text{Gal} / \sqrt{\text{Hz}}$ . [9]. This MEMS gravimeter is promising for future gravimetry because of its small size and affordable price. For current applications, the substantial drifts constitute a serious problem. 1.5 shows the relation between commercial relative gravimeters to their specifications

Table 1.3: Compared retail relative gravimeters to their stated specifications

Model Parameter	CG5 & CG6 Scintrex	gPhoneX Gravity Meter	iGrav	MEMS
Principle	Fused quartz spring	Zero-length spring tension	Superconducting	MEMS flexure spring
Measurement rate(Hz)	6/10		1	0.03
Sensitivity (mGal)	0.005	0.001	$10^{-6}$	0.01
Resolution ( $\mu\text{Gal}$ )	1	0.1	0.001	
Noise( $\mu\text{Gal} / \sqrt{\text{Hz}}$ )		0.1 to 0.3	0.3	40
Residual Drift( $\mu\text{Gal} / \text{day}$ )	20	1500	0.5	150
Volume(L)	15		104	0.2
Power Consumption(W)	10	300	1.3kW	
Mass(kg)	8.9	58	40	
Reference	[12]	[13]	[14]	[15]

### 1.3.2 Absolute Gravimeter

In the 1960's, a new generation of gravity instruments was invented, the absolute gravimeter. It keeps track of an object's free fall's duration and distance. In the free-falling technique, the used mass may be either launched or catapulted. Their basic method involves comparing the light reflected from a stationary mirror to light reflected from a falling mirror while using a laser beam as a reflection. By positioning the mirrors so that they form separate arms of an optical interferometer. The interference among the two distinct

beams of light allows for an accurate calculation of the differential acceleration of the two mirrors. Estimating the basic acceleration variables of time and distance is necessary for calculating absolute gravity than others. This kind of gravimeter is portable and stable in length, it can precisely measure the distance. Based on the ballistic trajectory, free-fall type gravimeters can be divided into direct free-fall and identical rise-and-fall kinds. The direct free-fall technique has the advantage of being more mechanically simple, which increases the data rate while the proportional rise-and-fall method is a little sensitive to some systematic racket[16]. An example of this kind of gravimeter is frequently used and commercially obtainable **Micro-g LaCoste FG5** and its elevated variant, the FG5-X.[17] which is shown in 1.4

It is operated on a Michelson interferometer. To calculate the test mass's distance trav-

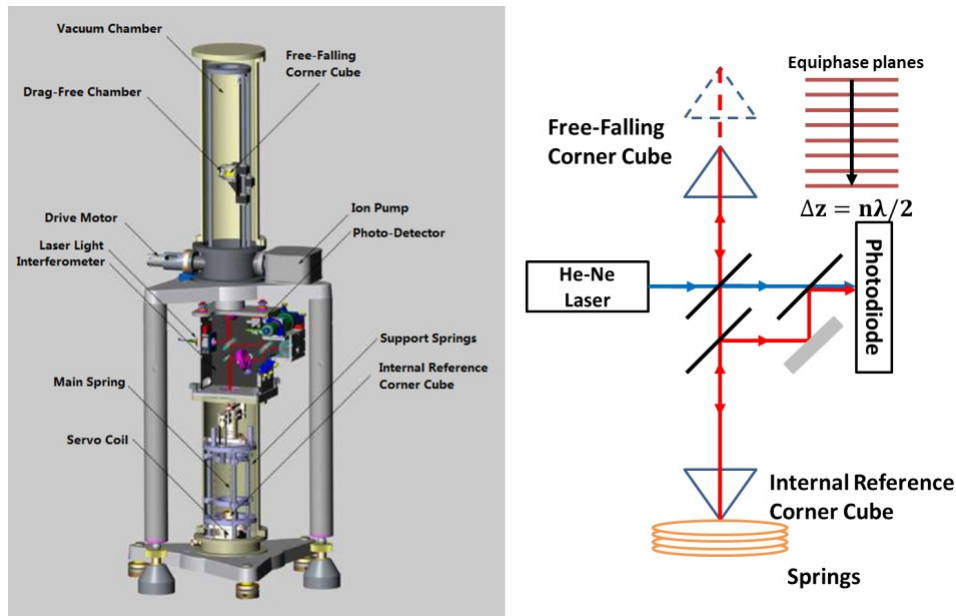


Figure 1.4: Principle of Absolute Gravimeter: FG5 [17]

eled during a period of time  $T$ , corner cubes types mirrors are used. The other mirror serves as a reference, while one is fixed. In the presence of gravity, the other corner cube moves upward direction. Measurement of  $g$  is obtained by counting the optical interference fringes that pass through the freely moving second corner of the cube. Based on absolute wavelength standards, optical fringes offer a very accurate method of measuring distance. The **IMGC** is another comparable design of absolute gravimeters. It's based on the symmetrical rise-and-fall method and it follows the same principle of **FG5**, with the exception that the beam splitter and the mirrors are integrated into a single, plane-parallel glass plate[18]. These instruments are extremely accurate, with a few  $\mu\text{Gal}$  levels of precision.

Atoms have been discovered to be a good alternative to a macroscopic mass for use as the test mass in free-fall gravimeters. In 1991, famous scientists Mark Kasevich and Steven Chu performed the first demonstration of a cold atom gravimeter which had a resolution of  $30\mu\text{Gal}$  after 2000 s of integration time [21]. Since then, numerous institu-

Table 1.4: Comparison of the absolute gravimeters' with listed parameters in the industrial market

The specifications	FG5 & FG5X	A10	AQG
Working Principle	Free-fall corner cube	Free-fall corner cube	Atom interferometry
Accuracy( $\mu\text{Gal}$ )	2	10	A few
Exactness( $\mu\text{Gal}/\sqrt{\text{Hz}}$ )	15	100	50
Long-term strength			1 $\mu\text{Gal}$
The rate of Measurement	a couple of seconds		2Hz
Consumption of Power(W)	500	300	300
Mass(kg)	320	105	100
Reference	[19]	[16]	[20]

tions around the world have been researching the sensitivity and safety of these sensors. Due to improvements in robustness and compactness, atomic gravimeters show promise for use in the field. Atomic gravimeters can achieve measurement rates that are comparable to relativistic gravimeters and are more compact than corner cubes. Table 1.4 shows the comparison of the recent commercial gravimeter to the relative gravimeter with their specifications.

### 1.3.3 Atom interferometric-based gravimeters

The first step is to figure out the workings method of the atom interferometry gravimeter, here describe the principle. In today's research field, there are numerous use of atom interferometry principles. Currently, atom-based gravimeters mostly use the mechanism of the light-pulse atom interferometry principles for measuring gravity [21]. Chapter 2 explains the detailed theory. The mechanism of the light-pulse atom interferometer is similar to the methodology of the Mach-Zehnder type optical interferometer shown in Figure 1.5. In an optical interferometer, a beam of light is split into two different pieces by a beamsplitter, deviated by mirrors, and then combined again by a second beamsplitter. The phase shift gathered between the interferometer's arms during propagation can be specified by counting the intensity at the output ports [22]. Using Raman laser pulses this scheme [splitting-redirect-recombination] is applicable in Atom interferometer [21].

#### 1.3.3.1 Working Principle

The most fashionable measurement method uses a Mach-Zehnder-type interferometer that is based on freely falling atoms reacting with light pulses[21]. The principle of this type of interferometer is shown in 1.6. Assuming all atoms are in ground state  $|g\rangle$  After applying the First Raman pulse  $\frac{\pi}{2}$  on the atomic wavepacket, it split two states, and the atoms are equally populated in these two states ground state  $|g\rangle$  and excited state  $|e\rangle$ . After some duration( $T$ ) when an atom interacts with  $\pi$ -pulse then it obtains a phase  $\phi_2$  and the population of the states are exchanged. After a second free evolution  $T$ , the



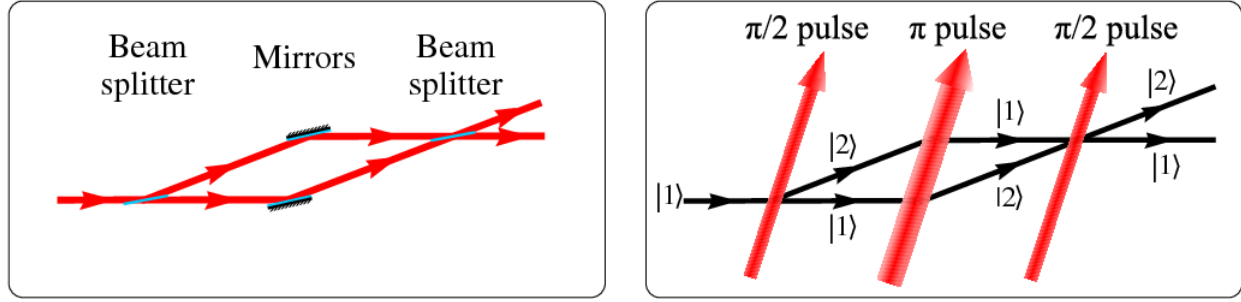


Figure 1.5: Sequence of three laser pulses to form Mach-Zehnder interferometer. (Left: Light interferometer), (Right: Atom interferometer). [22]

atomic clouds overlap. Atom interacts with 3rd i.e 2nd  $\frac{\pi}{2}$  pulse, the two atomic clouds are combined. All atoms obtain a phase  $\phi_3$  from the second  $\frac{\pi}{2}$  pulse. Here  $\frac{\pi}{2} - \pi - \frac{\pi}{2}$  sequence works as a **beam splitter-Mirrors-beam splitter**. First  $\frac{\pi}{2}$  works as a splitter, splitting the states with a velocity difference  $v = \frac{\hbar k}{m}$ . Where  $\mathbf{k}$  is the wave vector and  $\mathbf{m}$  is the mass of the atom. The population distribution between the two states is equal at the output with no path disruption.

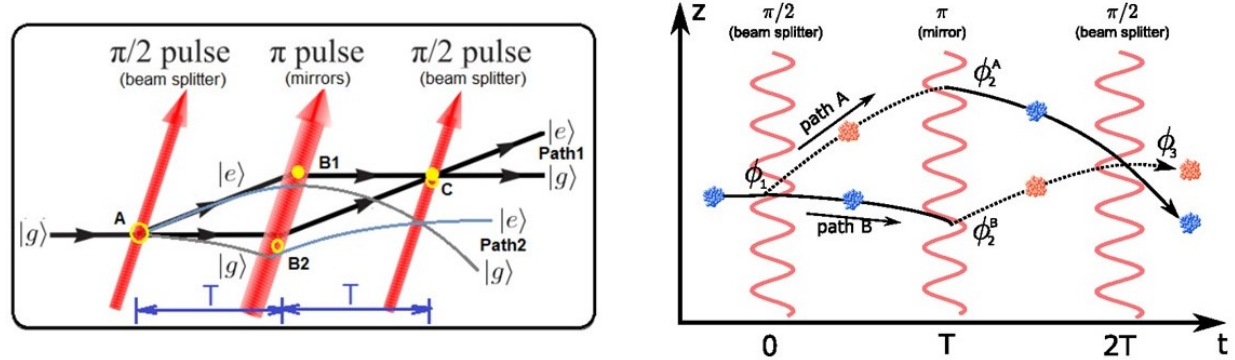


Figure 1.6: Schematic of atom interferometry principle: It works Three Raman pulses  $\frac{\pi}{2} - \pi - \frac{\pi}{2}$ . First pulse responsible for superposition between two states ( $|g\rangle, |e\rangle$ ) with different momenta. The second and third pulses reflect the trajectories and close the interferometer[21]

The probability distribution of the atom in the excited state  $|e\rangle$  which depends on the dephasing is,

$$P = \frac{1}{2}(1 - \cos \Delta\Phi) \quad (1.12)$$

The probability distribution of the atom i The probability distribution of the atom i Where  $\Delta\Phi$  is the phase difference. In an atom interferometer, there occurs two types of phase

shifts one is an acceleration phase shift and the other is an interferometric phase shift.

$$\Delta\phi = \mathbf{k} \cdot \Delta\mathbf{z} + \int_0^T \delta(t) dt \quad (1.13)$$

$\delta z$  is the traveled distance of the atom according to the path.  $\delta(t)$  detuning of the laser during interrogation time  $T$ . The interferometric phase shift in the gravity field during the free-fall time,

$$\Delta\phi = kgT^2 \quad (1.14)$$

where  $g$  denotes the earth's gravitational acceleration and we assume that the laser frequency precisely matches the resonance of the atoms. In fact, the Doppler effect during atom free fall can produce frequency detuning. The frequency of the laser is chirped during the interferometry sequence to account for this phase shift. From equation 1.14 the Sensitivity depends on  $T^2$ . This measuring approach allows for extremely stable absolute measurements since it only depends on the characteristics of the atoms in free fall and their interaction with precisely timed and frequency-controlled light fields. Its produced long-term stability.

### 1.3.3.2 The Gravimetric Atom Interferometer

The GAIN experiment is an atom interferometer that was created to provide highly accurate gravity measurements at various sites. Compared to optical laboratory tests, this field of application involves stronger and somewhat novel requirements. To obtain a transportable sensor, many pieces, particularly for the laser setup, have been completely reworked to substantially reduce their size. When something is described as being transportable, it can be driven on wheels to the desired site by a small truck. Because of its portability, sensitivity, and stability, this gravimeter has shown to be a more effective tool in numerous kinds of geophysical applications.

## 1.4 Applications

In the fields of geodesy, geophysics, and metrology, gravity observations are an important tool. Geodesy is the study of the Earth's shape and how gravity affects it. Here, the so-called geoid, which corresponds to the mean sea level and represents an equipotential surface in the gravity field, is utilized as a height reference. It is specifically used in navigation and mapping to determine elevation. Additionally, studies of oceanic currents, changes in the mean sea level, and hydrology all depend on knowing the specific morphology of the area. Geophysics specifically looks for anomalies in the gravity field. They provide details on the Earth's mass distribution and mass movement, providing insight into the planet's geological structure and geodynamics. For instance, specific structures are frequently linked to the discovery of oil and gas. Processes like plate tectonics, volcanism, and mountain-building are all examples of geodynamics. The land uplift brought on by post-glacial rebound is another consequence that can be seen. The local gravity value



is necessary in metrology, for example, for force and pressure measurements that are used to calibrate pressure gauges or redefine the kilogram standard.

This mobile quantum gravimeter is ideal for fieldwork, and thus, geophysical investigations as well. From the perspective of geophysics, the small cold atom quantum gravimeter is perfect for absolute measurement of gravity fluctuations due to its portability, high sensitivity, improved stability, and precise measurement like VOLCANO ERUPTIONS [23], Monitoring glaciers[24], Detection of tunnel beneath the ground [25], etc.

The requirements for accuracy vary depending on the application, and it is generally necessary to distinguish between relative and absolute accuracy as well as time resolution (sensitivity). For the monitoring of geodynamical processes, for example, the requirements can be as high as  $10^{-8}g$  to  $10^{-10}g$  in relative accuracy and  $10^{-9}g$  in absolute precision for applications in metrology, for example.

## 1.5 Use Atom Interferometry(AI) principle

We witnessed the emergence of a new generation of inertial sensors throughout the 28-year-long development of atom interferometry. Both The scientific community as well as the industry are researching and developing accelerometers, gravimeters, gyroscopes, and gradiometers. The atom interferometer's performance has recently been steadily improved, and work has been done to expand its use in other disciplines. Long baselines [26], big momentum transfer [27], and innovative schemes [28] have all shown high sensitivity. In order to improve the sensitivity, atom interferometry in microgravity has been suggested, particularly for fundamental tests like the viability of the Einstein equivalence principle [29].

Aside from gravity, atom interferometers have been shown to have the highest level of accuracy in the lab for rotation [30] and gravity gradients [31]. The applications, such as in oil exploration, inertial navigation, or geodesy[32], are extremely attractive due to the atomic sensors' extraordinary sensitivity and virtually drift-free nature. The fine structure constant [8], the SI unit of mass [33], the Newtonian gravitational constant[34], and the weak equivalence principle [35] have all been calculated using atom interferometers in fundamental research. Applications in the future might involve finding gravitational waves[36] or dark energy [37].

## 1.6 Layout of the Thesis

The purpose of this thesis is to attempt to communicate the understandings that have been developed through theoretical models and data analysis for the identification of the subsurface. It represents a novel technique for object detection as well as precision of gravity using 1-D gravimeter. This investigation provides insight into how gravity signals alter during activity caused by subsurface materials. The cold atom-based gravimeter's theoretical underpinnings would be provided by this study. It examines the sensitivity of a portable quantum gravimeter, which is required for geophysical surveys to determine changes in subsurface gravity. After that, systematic errors are studied in gravity sig-

nals, and the error resulting from these systematic effects is estimated. For the quantum gravimeter to have improved sensitivity and high precision, it is being studied how to reduce these inaccuracies caused by systematic influences. This research will be helpful in actual field geophysical surveys and in the detection of various materials that could be present underground. Before going to study in the field, it will assist in creating a plan. The organizing of this thesis is,

**Chapter2** Theory of an atom interferometry hypothesis is presented. It gives the relationship between the experiment's measured phase and the atoms' acceleration.

**Chapter3** defines the theory and calculation of efficient models which help to determine the gravitational acceleration, tensor, mass, and location of the object.

**Chaper4** This chapter shows the numerical results computed using Python language. In the appendix part theoretically calculate the expected mass of the anomaly.

# Chapter 2

## Background Theory

Quantum Gravimeter based on Raman atom interferometry principle. It works in a sequence of three Raman light pulses which act on the cloud of laser-cooled atoms in free fall. Laser cooled, this term is surprising. Normally a strong laser is produced a heating effect compared to cooling. For producing the Laser-cooling technique we must follow a restricted range of conditions with laser frequency close to the resonance frequency in an atomic transition. Here I discussed briefly the factors which are involved to achieve the temperature of the laser cooling method and the path to complete the experiment.

### 2.1 Cold Atoms

From **equipartition of energy** theorem, thermal velocity in one dimension is,

$$\bar{v} = \frac{\sqrt{k_B T}}{m} \quad (2.1)$$

From equation 2.1 the average velocity depends on the temperature( $T$ ) and mass( $m$ ) of the atom.  $k_B$  is the **Boltzmann** constant. It is clear that heavy atoms have lower velocities. By declining the intermediate velocity of the thermal atoms to only a short of while  $mm/sec$ , Only a few  $K$  degrees of temperature can define groups of atoms. The temperature for a single atom cannot be precisely determined. Since the Maxwell-Boltzmann distribution is used to determine the temperature, using the average velocity formula we estimate the temperature of the atomic cloud. It is possible to reach temperatures proportionate to the recoil velocity using typical laser cooling techniques, giving a minimum thermal velocity. From the location where it was cooled and trapped., an atom will only move a few millimeters. Thus, throughout the duration of an experimental sequence, atom ensembles can stay localized. The famous striking effects **Bose-Einstein condensate (BEC)** Consequently, at a lower temperature, the group of atoms behaves as a single wavefunction. In order to create atomic ensembles of millions of atoms that are cooled to a few  $\mu K$  cold atoms have been created utilizing the conventional mix of background vapor loading, 3D magneto-optical trapping, and optical molasses. In a thermal atomic cloud, the typical densities of the atoms are in order of  $10^{10} cm^{-3}$  [38], with small atom-atom collision. The cold atoms are ( $^{87}Rb$   $^{133}Cs$ , etc) more useful than the charged particle

or photons for realizing highly sensitive devices for inertial accelerometers and rotations. These atoms are less sensitive to perturbing the electric and magnetic fields. Since the magneto-optical trap (MOT) introduction is given for completeness even though this literature is well-documented and extensive in its details of the trapping and cooling approaches.

### 2.1.1 Optical Molasses and MOT

Optical Molasses is the laser-cooling technique along one direction which is created using two counter-propagating lasers. This arrangement is shown in figure 2.1. Here atom moves with very small velocities along the  $\pm X$  direction. But it has no impact on their mobility in the  $y$  and  $z$  dimensions and is unable to trap them at the same location in space. To trap the atom at the same position in space for each of the three velocity components (i.e., the  $\pm x$ ,  $\pm y$ , and  $\pm z$  directions) we require a **Magneto-optical trap** system.

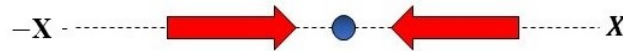


Figure 2.1: Optical Molasses effect: Two counter-propagating laser used [38]

Figure 2.2 illustrates the most common type of magneto-optical trap, which consists of a six-beam configuration with a magnetic quadrupole field. An optical molasses effect is created for all three coordinates by the three pairs of orthogonal counter-propagating beams. The magnetic quadrupole consists of two coils conveying opposing-flowing currents. This quadrupole field makes an attractive potential for atomic states. In a magneto-optical trap (MOT), which is an extension of laser cooling, an atom travels with a relative velocity to a laser beam that is detuned from resonance. This velocity encounters a scattering force corresponding to its velocity vector.

Three orthogonal duos of beams that have been detuned below the resonant frequency—a process known as red detuning—intersect at the magnetic zero of a quadrupole field to form a three-dimensional MOT. Atoms moving with the suitable choice of circular polarisation through the beams exert a force that is directed towards the central region of the trap, where the magnetic field is zero. With respect to the center of the trap space, the magnitude of the force changes with the position and velocity of the atoms. When atoms move towards one of the beams, the light detuned from the atomic resonance is scattered. Then the frequency of Doppler shifting is more relative to the resonance frequency. The resonant frequency is shifted positionally by the magnetic field, which increases the scattering force as one moves away from the trap center. The atom must undergo several scattering incidents in order to lose its kinetic energy, which cools it down and causes it to drift toward the center of the trap until the rate of scattering from all directions is similar. Without taking into account sub-Doppler cooling [39] this indicates the Doppler limit, when the scattering force is equivalent to the heating from arbitrary emissions and absorption, yielding the lowest temperature possible in the laser cooling of atoms. The

MOT temperature( $T_D$ ) can be expressed as being of order the Doppler limit,

$$T_D = \frac{\hbar\Gamma}{2k_B} \quad (2.2)$$

Where  $\Gamma$  is the linewidth of the transition. Atoms that are slowed but reach the edge of the

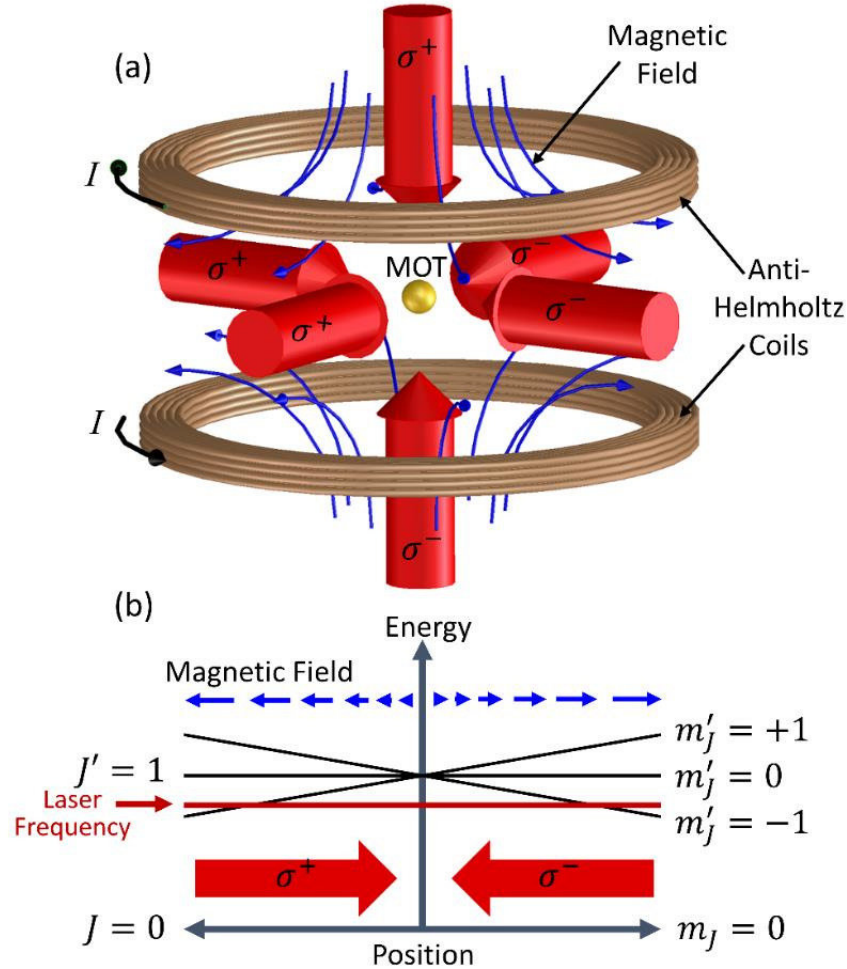


Figure 2.2: Magneto-optical-trap: The mechanism of the magneto-optical trap in the simplified scenario of an atom with a transition from  $|J\rangle = 0$  to  $|J\rangle = 1$  (a) The trap center, which is determined by the zero of a quadrupole magnetic field produced by a pair of coils with opposing currents (anti-Helmholtz coils), is targeted by three mutually orthogonal, counter-propagating couples of laser beams. (b) Schematic of Energy diagram along the one axis of the MOT.[39]

trapping region before stopping won't be captured because the trapping region is finite. The upper boundary of atomic velocity for which trapping will happen, the estimated

capture velocity [40] is,

$$v_c \approx \sqrt{\frac{\hbar k \Gamma D}{2m}} \quad (2.3)$$

Where  $D$  is the beam diameter. Direct trapping from background gases is possible due to the easy availability of atoms with thermal velocities below the capture velocity in room-temperature vapor, as opposed to injection from a slowed atom beam, which is typically produced from a 2D MOT.

MOTs have been an almost universal starting point for cold atom experiments for group 1 alkali and group 2 alkaline earth metals because they enable millions of atoms to be trapped in a few hundred ms and are constrained to a trap center of only a few mm. Now this mechanism has also been used to develop cold molecules [41] and sympathetically cool ions [42].

## 2.2 Raman transition with photon

Numerous methods can be used to implement matter-wave interferometers. Here, we demonstrate how an atom interferometer works when Raman transitions are driven. This technique permits effective separation, deflection, and recombination of the atomic wavepackets utilizing enormous momentum recoil, and it also enables reading out the interferometer using populations of atomic states. The effectiveness of atom-interferometry techniques via stimulated Raman transitions are invented by the substantial momentum

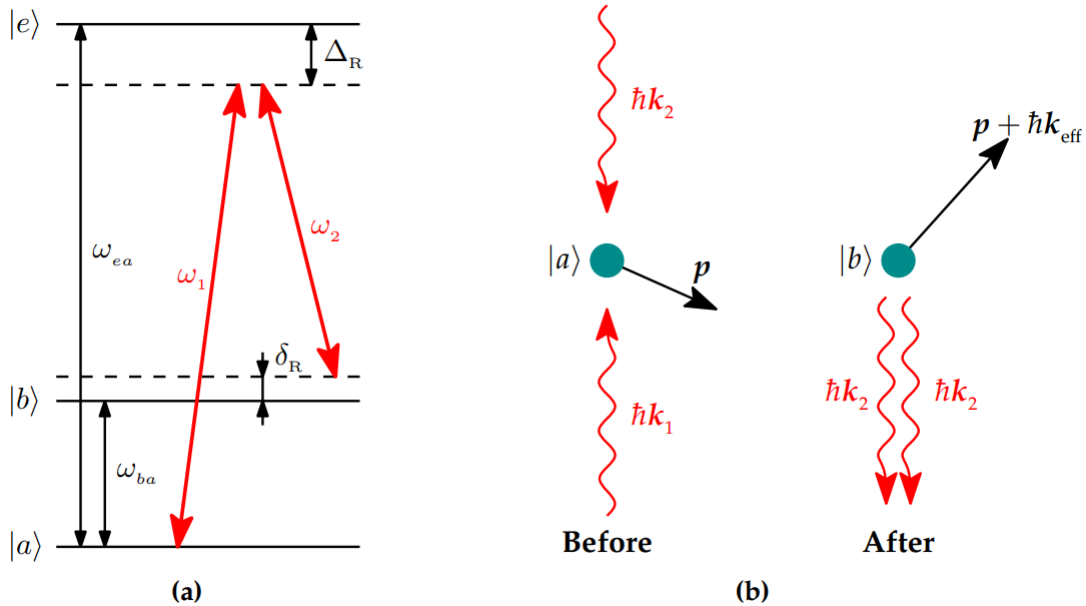


Figure 2.3: Schematic of Stimulated Raman transition (a) Internal energy level diagram of the atom (b) Momentum conservation in photon process[43]

recoil and the ability to combine stable atomic states. In a two-photon process called stimulated Raman- transitions, the two hyperfine ground states can be connected Here,

the two-photon mechanism illustrated in Figure 2.3 serves as the foundation for the atom interferometry experiment. Assume an atom with two long-lived states  $|a\rangle$  and  $|b\rangle$ . These two states are coupled by stimulated Raman transition. The hyperfine splitting of the two ground states is equivalent to  $w_{ba}$ .  $w_{ba}$  is the angular frequency in the order of GHz. Due to the fact that this is substantially shorter than visible wavelengths, two laser light fields are used to couple the states together. The stimulated Raman transition is driven by a single pair of counter-propagating lasers with optical frequencies  $w_1$  and  $w_2$ . These frequencies are separate from the close to the  $w_{ba}$  but the same as the optical transition for typical excited state  $|e\rangle$ . When an atom absorbs a photon of energy  $\hbar w_1$  from the first light field and  $\hbar w_2$  from the second light field i.e stimulated emission and reaches  $|b\rangle$  state from  $|a\rangle$  state. The light fields are detuned from the level separation  $w_{ea}$  to avoid excited state population and limit decoherence from spontaneous emission.

From energy conservation law which depicted Figure 2.3,  $\mathbf{p}$  is the momentum of the atom when the atom stays at  $|a\rangle$  state, and after absorption a photon imparts a momentum  $\hbar \mathbf{k}_1$ . Where  $\mathbf{k}_1$  is the wavevector for the first light field. Similarly for stimulated transition  $\hbar \mathbf{k}_2$  is the additional momentum for the second light field with wavevector  $\mathbf{k}_2$ . The effective wavevector between this two-photon transition  $\mathbf{k}_{\text{eff}} = \mathbf{k}_1 - \mathbf{k}_2$ . The two-photon resonance condition must be encountered in order to drive the Raman transition successfully. Due to the conservation of energy among those states, the exact resonance condition for Raman's transition is,

$$\hbar w_1 + \hbar w_a + \frac{|\mathbf{p}|^2}{2m} = \hbar w_2 + \hbar w_b + \frac{|\mathbf{p} + \hbar \mathbf{k}_{\text{eff}}|^2}{2m} \quad (2.4a)$$

$$w_1 - w_2 - w_{ba} = \frac{|\mathbf{p} + \hbar \mathbf{k}_{\text{eff}}|^2}{2m\hbar} - \frac{|\mathbf{p}|^2}{2m\hbar} \quad (2.4b)$$

The detuning is,

$$\delta_R = w_1 - w_2 - w_{ba} + \frac{|\mathbf{p}|^2}{2m\hbar} - \frac{|\mathbf{p} + \hbar \mathbf{k}_{\text{eff}}|^2}{2m\hbar} \quad (2.5)$$

$\delta_R$  is also known as two-photon detuning. The detuning from the excited state or one photon detuning is  $\Delta_R$ ,

$$\Delta_R = w_{ea} - w_1 + \frac{|\mathbf{p}|^2}{2m\hbar} - \frac{|\mathbf{p} + \hbar \mathbf{k}_{\text{eff}}|^2}{2m\hbar} \quad (2.6)$$

From equation 2.6

$$w_1 - w_2 = w_{ea} + \frac{\mathbf{p} \cdot \mathbf{k}_{\text{eff}}}{m} + \frac{\hbar \mathbf{k}_{\text{eff}}^2}{2m} \quad (2.7)$$

$$w_{12} = w_{ea} + w_D + w_{\text{rec}} \quad (2.8)$$

$w_{ea}$  denotes the hyperfine state splitting,  $w_D$  Doppler shift, and recoil shift define by  $w_{\text{rec}}$ . Only atoms moving within a certain range of velocities can contribute to the Raman transition because of the Doppler shift factor. This is the fundamental idea behind how we choose the velocity and further cool the atoms before the atom interferometer.

So from the above description, we may write three basis states with the corresponding energy( $\hbar w_i$ ) is

$$|a; \mathbf{p}\rangle \quad \hbar w_a = \frac{|\mathbf{p}|^2}{2m} \quad (2.9a)$$

$$|b; \mathbf{p} + \hbar \mathbf{k}_{\text{eff}}\rangle \quad \hbar w_b = \frac{|\mathbf{p} + \hbar \mathbf{k}_{\text{eff}}|^2}{2m} + w_{ba} \quad (2.9b)$$

$$|e; \mathbf{p} + \hbar \mathbf{k}_1\rangle \quad \hbar w_e = \frac{|\mathbf{p} + \hbar \mathbf{k}_1|^2}{2m} + w_{ea} \quad (2.9c)$$

These states can be represented in the new wavefunction with a slowly varying coefficient  $c_a$  shown in the next section. This theory approaches a semi-classical model where the atom behaves as a quantum object in a classical light domain.

### 2.2.1 Atom in three-level system

The wave function of an atom is a linear combination of all possible states with time-varying coefficients, whose square indicates the probability that the atom will be in that state at a given moment. In light of this, the wave distribution for the three-level system for a single momentum  $\mathbf{p}$  is

$$|\psi_p(t)\rangle = C_{a,\mathbf{p}}(t) |a; \mathbf{p}\rangle + C_{b,\mathbf{p}+\hbar\mathbf{k}_{\text{eff}}}(t) |b; \mathbf{p} + \hbar \mathbf{k}_{\text{eff}}\rangle + C_{e,\mathbf{p}+\hbar\mathbf{k}_1}(t) |e; \mathbf{p} + \hbar \mathbf{k}_1\rangle \quad (2.10)$$

In the absence of spontaneous emission, the evolution of the atomic states is controlled by the Hamiltonian.

$$\mathcal{H} = \frac{\hat{\mathbf{p}}^2}{2m} + \hbar w_{ba} |b\rangle \langle b| + \hbar w_{ba} |e\rangle \langle e| - \hat{\mathbf{d}} \cdot \mathcal{E}(\mathbf{r}, t) \quad (2.11)$$

$\hat{\mathbf{p}}$  is the momentum operator,  $\hat{\mathbf{d}}$  denotes the electric dipole operator. From equation 2.11 the last term represents the electric dipole approximation of the interaction between the atom and the light field.

The time-dependent Schrodinger equation is,

$$i\hbar \frac{d\psi(t)}{dt} = E\psi(t) \quad (2.12)$$

$E$  is the energy and  $\psi(t)$  is the time-dependent wave function. If we write the energy replaced by atomic state energy which controlled the Hamiltonian ( $\mathcal{H}$ ), in the momentum-dependent wavefunction,

$$i\hbar \frac{d\psi_p(t)}{dt} = \mathcal{H}\psi_p(t) \quad (2.13)$$

If we solved this equation 2.13 [43] then we introduced Rabi frequencies which defines in the next para.



### 2.2.2 Rabi Oscillation

Through interaction with the light field, the Rabi frequency expresses the coupling between each ground state and the intermediate state. It provides movement between states, which is based on both the characteristics of the light and the strength of the coupling between the two atomic states. The Clebsch-Gordan coefficients, which control the permitted transitions and relative coupling between states [44], can be used to calculate this coupling by reducing the dipole operator into a matrix. The Rabi frequencies are,

$$\Omega_1 \approx -\frac{\langle a | \hat{\mathbf{d}} \cdot \mathcal{E}_1 | e \rangle}{2\hbar} \quad (2.14a)$$

$$\Omega_2 \approx -\frac{\langle b | \hat{\mathbf{d}} \cdot \mathcal{E}_2 | e \rangle}{2\hbar} \quad (2.14b)$$

These represent the coupling of  $|a\rangle, |b\rangle$  to the excited state  $|e\rangle$  through the respective laser. In order to prevent spontaneous emission  $|\Delta| \gg |\delta|, |\Omega_1|, |\Omega_2|$ . So applying this condition to the coefficient of time-dependent oscillation is much less than to oscillation frequency ( $\Delta$ ).

The energy of each state changes due to atom-light interaction, i.e. called a light shift, or the a.c. Stark effect[45].

$$\Omega_{AC} \approx \frac{|\Omega_2|^2}{4\Delta} + \frac{|\Omega_1|^2}{4\Delta} \quad (2.15)$$

Due to the shifting of the light field, there produce frequency detuning  $\delta_{AC}$ , which represents

$$\delta_{AC} \approx \frac{|\Omega_2|^2}{4\Delta} - \frac{|\Omega_1|^2}{4\Delta} \quad (2.16)$$

It should be noted that by adjusting the Rabi frequencies of the two to be equal, the effects caused by the light shift can be eliminated. Adjusting the intensity ratio between the two frequencies can be accomplished practically. Additionally, the phase term  $\phi_{eff} = \phi_1 - \phi_2$ , derived from the light interaction, is used to calculate the effective Rabi frequency, which is the result of the two transition rates. The effective Rabi frequency,

$$\Omega_{eff} \approx \frac{\Omega_2 * \Omega_1}{2\Delta} \exp(i\phi_{eff}) \quad (2.17)$$

Rabi frequency in terms of light shifts and frequency detuning derivation is here[21]

$$\Omega_R \approx \sqrt{\Omega_{eff}^2 + (\delta - \delta_{AC})^2} \quad (2.18)$$

At  $t_0$  atom starts to move from the lower ground state, the probability coefficients are  $C_a(\mathbf{p}, t_0) = 0, C_b(\mathbf{p}, t_0) = 1$ . At  $t_0 + \tau$  the probability of finding the atom in individual state simultaneously respectively,

$$P_a(\mathbf{p}, t_0 + \tau) = |C_a(\mathbf{p}, t_0 + \tau)|^2 = \cos^2\left(\frac{\Omega_R}{2}\tau\right) + \frac{|\delta_{AC} - \delta_R \Omega_R|^2}{\sin^2}\left(\frac{\Omega_R}{2}\tau\right) \quad (2.19)$$

$$P_b(\mathbf{p}, t_0 + \tau) = |C_b(\mathbf{p}, t_0 + \tau)|^2 = \left| \frac{\Omega_{eff}}{\Omega_R} \right|^2 \sin^2 \left( \frac{\Omega_R}{2} \tau \right) = \left| \frac{\Omega_{eff}}{\Omega_R} \right|^2 \frac{1 - \cos \Omega_R \tau}{2} \quad (2.20)$$

The oscillations between this population of states  $|a\rangle$  and  $|b\rangle$ , generally this kind of oscillation called as **Rabi oscillations**[46], but here the oscillation frequency  $\Omega_R$  is the outcome of a two-photon shifting. Figure 2.4 Shows the Rabi oscillations at  $\tau = 0$  of the state  $|b\rangle$  from the state  $|a\rangle$  at different detuning ( $\delta_R$ ).

From probability transition equations(2.19,2.20) if  $\delta_R = \delta_{AC}$  and  $\Omega_R = \Omega_{eff}$  then their

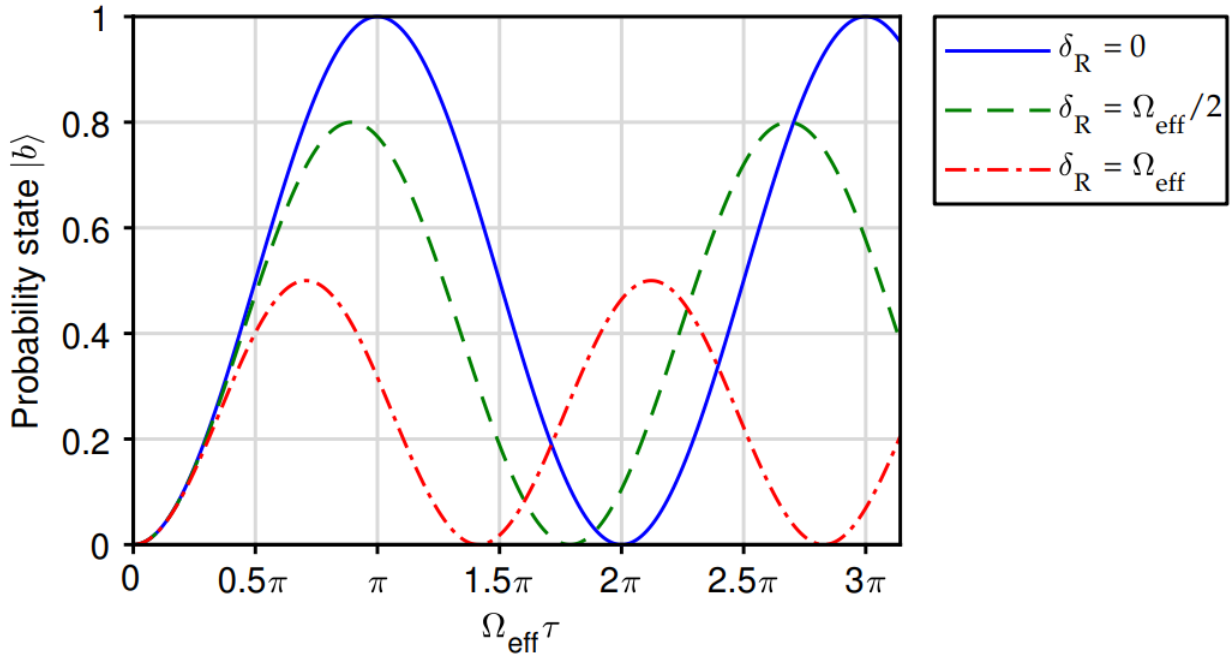


Figure 2.4: Rabi oscillations[47]

produce possibly a complete population transfer between the states. This indicates that detuning from the resonance state would compensate for the differential light shift resulting from the AC-Stark effect[47]. By balancing the laser intensities in such a way that the equation's 2.14 Rabi frequencies are equal,  $\delta_{AC}$  could be driven to disappear. This is standard procedure in atom-interferometry studies because it makes it attainable to perform a successful stimulated Raman transition on resonance. Therefore, it is assumed that  $\delta_{AC} = 0$  for the remainder of this chapter.

From equation 2.20 after time the largest population transfer occurred when

$$\tau_\pi = \frac{\pi}{\Omega_{eff}} \quad (2.21)$$

which plotted in figure 2.4. As a result, a laser pulse with this characteristic time is commonly referred to as a " $\pi$ -pulse." By applying a half  $\frac{\pi}{2}$ -pulse to the atom, it is possible to get it into an equal superposition of states then,

$$\tau_{\frac{\pi}{2}} = \frac{\pi}{2\Omega_{eff}} \quad (2.22)$$

This  $\frac{\pi}{2}$ - pulse works as a beam splitter for the atom whereas a  $\pi$ -pulse switches its present state. In comparison to an optical mirror, the latter is also referred to as a matter-wave reflector or mirror pulse. This technique uses Raman pulses—a type of laser pulse that drives stimulated Raman transitions—to establish an atom interferometer.

### 2.2.3 Mach-Zehnder Atom interferometry - 3 pulse schemes

This interferometry follows this scheme ( $\frac{\pi}{2} - \pi - \frac{\pi}{2}$ ) which discuss in the introduction part, here describes how 3-pulses works as a beam splitter and mirror that's why we say atom interferometry is analog of optical Mach- Zehnder interferometer. If  $\delta \ll \Omega_{eff}$ ,  $\Lambda \rightarrow 1$  equation 2.19, 2.20 maybe write as,

$$|C_a|^2 = \frac{1}{2}(1 + \cos(\Omega_{eff}\tau)) \quad (2.23)$$

$$|C_b|^2 = \frac{1}{2}(1 - \cos(\Omega_{eff}\tau)) \quad (2.24)$$

where  $\Lambda = |\frac{\Omega_{eff}}{\Omega_R}|^2$  is the population oscillation. This equation 2.23 apply in two special case,

- **$\pi$ -pulse as a Mirror**

An atom interacts with our light pulse in the ground state  $|a\rangle$ ,  $|C_a|^2 = 1$ . when the largest population occurs then their probability of coefficient is by using equation 2.21. The population in the excited state at  $|b\rangle$  at  $\tau_\pi$  is

$$|C_b|^2(\tau_\pi) = 1 \quad (2.25)$$

while The population in the ground state at  $\tau_\pi$  time is zero ( $|C_a|^2(\tau_\pi) = 0$ ).

This indicates that the entire atomic population has been successfully switched from one hyperfine state to the other. This suggests that the atom in the excited state —ei has changed direction, creating a path spatially distinct from its initial trajectory and acting as a mirror on the wave packet because we also correlate the momentum state with our internal state.

- **$\frac{\pi}{2}$ -pulse as a beam splitter**

At time  $\tau_{\frac{\pi}{2}}$  from equation 2.22 the probability coefficient in the excited state ( $|b\rangle$ ) is,

$$|C_b|^2(\tau_{\frac{\pi}{2}}) = \frac{1}{2} \quad (2.26)$$

also the population in the ground state  $|a\rangle$  is, ( $|C_a|^2(\tau_{\frac{\pi}{2}}) = \frac{1}{2}$ ) In this situation, we have produced two spatially separated paths, one for each atomic state, and a superposition of the two states, ( $|a\rangle$ ) and ( $|b\rangle$ ). The phenomenon relates to how an optical beam splitter splits a single input into two different outputs.

Now that we have a mirror and a beam splitter pulse, we are ready to build an atom interferometer. Two beam splitters and two mirrors are required for an optical Mach-Zehnder interferometer. By utilising the proper series of pulses, we may accomplish the same type of configuration with atom interferometry. From figure 1.6  $\frac{\pi}{2}$  pulse separate the two arms,  $\pi$ -pulse to reflect then complete the sequence with a  $\frac{\pi}{2}$ -pulse to recombine the atomic clouds. By computing the difference in laser phase that has accumulated over time between the two arms, we can estimate the phase in one of the interferometer's output ports:

$$\Delta\phi_{3P} = (\phi_1 - \phi_2) - (\phi_2 - \phi_3) = \phi_1 - 2\phi_2 + \phi_3 \quad (2.27)$$

Here introduce the sign conventions; if the ground state is the starting state this is a positive phase shift  $+\phi$ . On the contrary, when the light pulses on the excited state phase are negative,  $-\phi$

### 2.2.4 Phase shift for a constant acceleration

In the last section, we described how we could separate the two wave packets in space and simultaneously produce a superposition of atomic states. As we have seen, the separation depends on both the effective momentum exchanged and the interval between each pulse of light. The sensitivity of the interferometer to "inertial" forces increases if the distance between the two wave packets increases. We may generalize the expression for the phase shift as follows for the scenario of a three-pulse MachZehnder under a constant acceleration field  $\vec{g}$ :

$$\phi_g = k_{eff} \cdot \vec{g} T^2 \quad (2.28)$$

## 2.3 summary

From equation 2.28 the phase changes for gravity and the duration. Since  $\vec{g}$  is the tensor it has nine components, but for one-dimensional Quantum sensors like cold atom gravimeter is impossible to provide the whole tensor components. Since the primary goal is object detection using a gravimeter with precise gravity, I believe my thesis work is very applicable in the real field which is discussed in the next chapter.

# Chapter 3

## Towards an efficient Model

### 3.1 Work flow

Our main is to precisely measure the gravity and detect the mass. For this work, we used some models. The first step is to forwardly calculate the vertical gravity anomaly  $g_z$  by using the right rectangular prism model[48] [49]. Then compute the  $g_x, g_y$  and nine tensor components of gravity as a function of  $g_z$  in the Fourier domain using the Fourier model [50]. Now using those components in the Inverse model[51], we can estimate the mass and location of Unknown or known objects.

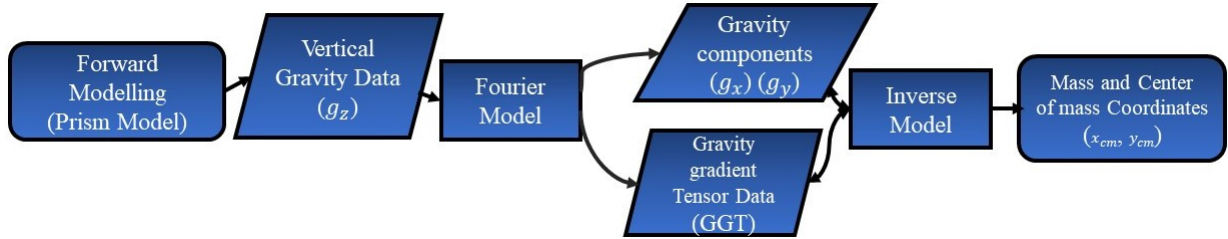


Figure 3.1: Work Flow

### 3.2 Forward Model

In general, Gravity and gravity gradient data are used to investigate subsurface geology based on mass distribution in the subsurface. As a result, estimating model parameters that emerge from etiological sources including position, variation of per unit volume, thickness, size, shape, extension, change of depth, and so forth is extremely crucial during the interpretation stage. It was difficult to explain the fairly-known perplexing in nature using the full tensor method of gravity, with compare to the gravity alone system. There are several ways to solve three-dimensional density problems. According to the fundamental geometrical paradigm, the bulk of right-handed rectangular prisms, the heap of polygonal prisms, and the other polyhedrons are the three most well-known categories.

To obtain the gravity attraction components and components of the spatial derivative of gravitational attraction many models are used as a forward model, among them Right rectangular prisms model is more used. Many researchers are worked on this model, to improve this. In the beginning, many people derive the spatial derivatives of the gravitational potential but this equation is partially correct. A brief discussion showed next for the variance of the formula of a gravitational attraction along  $z$ – direction.

### 3.2.1 Right rectangular prisms model

We have to take **right rectangular prisms model** as a forward model to calculate the vertical gravity data. The rectangular prisms model method is a simple way of estimating the volume of a mass. Every prism may be assumed to have a static density if it is small enough. Using the superposition principle, we can obtain the gravity anomaly at any point of the body that could be approximated by adding the effects of all the prisms. From Figure ?? the gravity calculate due to the prismatic body,

$$g(x, y, z) = -G \iiint \rho(\xi, \eta, \zeta) \frac{z - \zeta}{r^3} d\xi d\eta d\zeta \quad (3.1)$$

where,  $G$  is the universal constant of Gravity,  $\rho(\xi, \eta, \zeta)$  is the concentration of the body, and  $r$  is gap between field space to object space.

$$r = \sqrt{(x - \xi)^2 + (y - \eta)^2 + (z - \zeta)^2} \quad (3.2)$$

From equation 3.1 If we calculate the component of first-order derivatives of the gravitational potential at point  $(x, y, z)$  with limits  $\xi_1 \leq \xi \leq \xi_2$ ,  $\eta_1 \leq \eta \leq \eta_2$ ,  $\zeta_1 \leq \zeta \leq \zeta_2$

$$g = -G \int_{\xi_1}^{\xi_2} \int_{\eta_1}^{\eta_2} \int_{\zeta_1}^{\zeta_2} \rho(\xi, \eta, \zeta) \frac{z - \zeta}{r^3} d\xi d\eta d\zeta \quad (3.3)$$

After derived equation 3.3 by Sorokin (1951, p.370, equation(426)) the form of vertical  $g_z$  is

$$g_z = -G\rho \sum_{i=1}^2 \sum_{j=1}^2 \sum_{k=1}^2 \mu_{ijk} [x_i \ln(y_j + r_{ijk}) + y_j \ln(x_i + r_{ijk}) + z_k \arctan(\frac{x_i y_j}{z_k r_{ijk}})] \quad (3.4)$$

Many authors worked on this and get a different form of this equation, but the equation satisfies all conditions and it is suitable for writing. Thence from equation 3.5 is used for three-dimensional modeling. after derivation [48] [49] we get vertical component of gravity anomaly

$$g_z = -G\rho \sum_{i=1}^2 \sum_{j=1}^2 \sum_{k=1}^2 \mu_{ijk} [x_i \ln(y_j + r_{ijk}) + y_j \ln(x_i + r_{ijk}) - z_k \arctan(\frac{x_i y_j}{z_k r_{ijk}})] \quad (3.5)$$

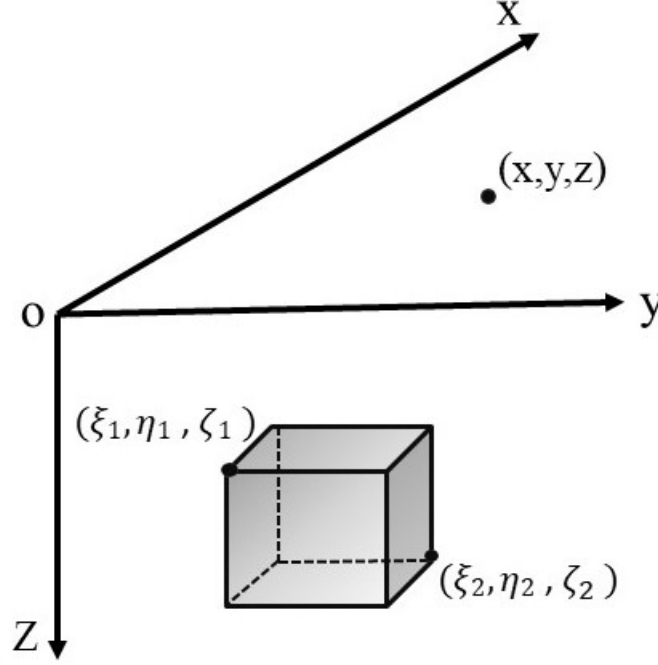


Figure 3.2: The right rectangular prism[52]

where  $\mu_{ijk} = (-1)^{(i+j+k)}$ ,  $r_{ijk} = \sqrt{x_i^2 + y_j^2 + z_k^2}$

$$x_i = x - \xi_i \quad (3.6)$$

$$y_i = y - \eta_i \quad (3.7)$$

$$z_i = z - \zeta_i \quad (3.8)$$

Using the Forward model calculation, the gravitational attraction along the x and y directions is,

$$g_x = -G\rho \sum_{i=1}^2 \sum_{j=1}^2 \sum_{k=1}^2 \mu_{ijk} [y_j \ln(z_k + r_{ijk}) + z_k \ln(y_j + r_{ijk}) - x_i \arctan(\frac{y_j z_k}{x_i r_{ijk}})] \quad (3.9)$$

$$g_y = -G\rho \sum_{i=1}^2 \sum_{j=1}^2 \sum_{k=1}^2 \mu_{ijk} [z_k \ln(x_i + r_{ijk}) + x_i \ln(z_k + r_{ijk}) - y_j \arctan(\frac{z_k x_i}{y_j r_{ijk}})] \quad (3.10)$$

To estimate the density or susceptibility structure of the earth, a new and promising way is a calculation of the gravitational potential of the anomalies. since gravity is a vector, so gravity gradient is a third-order tensor, due to symmetrical or irrotational attributes it has six independent components,  $(T_{xx}, T_{yy}, T_{zz}, T_{xy}, T_{xz}, T_{yz})$ .

For right rectangular prism synthetic equations for the six gravity gradient components

using equation (3.5, 3.9, 3.10) [53]

$$T_{xx} = G\rho \sum_{i=1}^2 \sum_{j=1}^2 \sum_{k=1}^2 \mu_{ijk} \arctan\left(\frac{y_j z_k}{x_i r_{ijk}}\right) \quad (3.11)$$

$$T_{yy} = G\rho \sum_{i=1}^2 \sum_{j=1}^2 \sum_{k=1}^2 \mu_{ijk} \arctan\left(\frac{x_i z_k}{y_j r_{ijk}}\right) \quad (3.12)$$

$$T_{zz} = G\rho \sum_{i=1}^2 \sum_{j=1}^2 \sum_{k=1}^2 \mu_{ijk} \arctan\left(\frac{x_i y_j}{z_k r_{ijk}}\right) \quad (3.13)$$

$$T_{xy} = -G\rho \sum_{i=1}^2 \sum_{j=1}^2 \sum_{k=1}^2 \mu_{ijk} \ln(z_k + r_{ijk}) \quad (3.14)$$

$$T_{xz} = -G\rho \sum_{i=1}^2 \sum_{j=1}^2 \sum_{k=1}^2 \mu_{ijk} \ln(y_j + r_{ijk}) \quad (3.15)$$

$$T_{yz} = -G\rho \sum_{i=1}^2 \sum_{j=1}^2 \sum_{k=1}^2 \mu_{ijk} \ln(x_i + r_{ijk}) \quad (3.16)$$

### 3.2.2 Drawbacks

So, after studying this model theoretically and computationally we observed that this method will help us to detect noise-free signals in any subsurface location. This model involves estimating the mass and location of any kind of heavy object. But this model does not suitable for the detection of a point mass[51]. Since the derivation of this mechanism is so lengthy and time-consuming to only detect the underground or on-ground object that is why we chose another model. This model helps us to determine the full gravity gradient whose tensor components are from a single vector component of gravity anomaly along the  $z$ – direction. The detailed theory is discussed in the next section.

## 3.3 The Fourier Model

The Fourier model is one of the novel techniques in geophysics application. If we detect known or unknown objects this method plays a significant role. Using this model we can estimate not only the nine gravity gradient tensor components but also determine the gravitational acceleration of the two horizontal components [50]. Those components help obtain the value of the expected mass.

Three gravity components obtained are continuous and differentiable in nature of the real stuff  $(x, y, z)$ , so the gravity is

$$\vec{g}(x, y, z) = g_x(x, y, z)\hat{i} + g_y(x, y, z)\hat{j} + g_z(x, y, z)\hat{k} \quad (3.17)$$

on a plain surface in the  $(x, y)$  if the vertical component ( $g_z$ ) is measured then the gravity is  $g_z(x, y, z_0)$ . Since, the potential  $\phi(x, y, z)$ , is a harmonic operation, it follows Laplace's



equation  $\nabla^2\phi(x, y, z) = 0$ . Again  $\vec{g} = -\vec{\nabla}\phi(x, y, z)$

$$\vec{\nabla} \cdot \vec{g} = 0 \quad (3.18a)$$

$$\vec{\nabla} \times \vec{g} = 0 \quad (3.18b)$$

After Fourier transform of Laplace's equation  $\nabla^2\phi(x, y, z) = 0$  [54],

$$F\{\nabla^2\phi\} = (k_x^2 + k_y^2 + k_z^2)\phi(k_x, k_y, k_z) = 0 \quad (3.19)$$

In 2 - D plane,  $|\mathbf{k}| = -ik_z = \sqrt{k_x^2 + k_y^2}$  where  $k_x, k_y, k_z$  are the reciprocal of spatial distances, wave vectors along different three axes  $x-, y-, z-$  direction. The Fourier transform pairs were established using the equation 3.18b, we obtain Fourier transform pairs,

$$\frac{\partial g_z}{\partial y} = \frac{\partial g_y}{\partial z} \leftrightarrow (-ik_y)G_z = |\mathbf{k}|G_y \quad (3.20a)$$

$$\frac{\partial g_x}{\partial z} = \frac{\partial g_z}{\partial x} \leftrightarrow |\mathbf{k}|G_x = (-ik_x)G_z \quad (3.20b)$$

$$\frac{\partial g_y}{\partial x} = \frac{\partial g_x}{\partial y} \leftrightarrow -ik_xG_y = -ik_yG_x \quad (3.20c)$$

so that  $g_x, g_y, g_z$  are the perpendicular elements of  $\vec{g}$  and  $G_x(k_x, k_y), G_y(k_x, k_y), G_z(k_x, k_y)$  are the two dimensional (2 - D) Fourier transform of  $g_x, g_y, g_z$ . From the above transformation relations equation (3.20),

$$g_i \leftrightarrow G_i = \frac{(-ik_i)}{|\mathbf{k}|}G_z(\mathbf{k}) \quad (3.21)$$

Where  $i = x, y,$

$$g_z \leftrightarrow G_z \quad (3.22)$$

### 3.3.1 Gravity Gradient Tensor Estimation

From the Forward model, we are familiar with how to derive gravity gradient tensor components. Basically, it is defined double derivative of the gravitational potential with respect to the location.  $g_{i,j}(\mathbf{x}) = \vec{\nabla} \mathbf{g}(\mathbf{x})$ . Where  $\mathbf{x} = (x, y),$

$$g_{i,j} = \begin{pmatrix} \frac{\partial g_x}{\partial x} & \frac{\partial g_x}{\partial y} & \frac{\partial g_x}{\partial z} \\ \frac{\partial g_y}{\partial x} & \frac{\partial g_y}{\partial y} & \frac{\partial g_y}{\partial z} \\ \frac{\partial g_z}{\partial x} & \frac{\partial g_z}{\partial y} & \frac{\partial g_z}{\partial z} \end{pmatrix} \quad (3.23)$$

These are the components of the two times of derivatives of potential, simply the entire matrix form of the gradient is equation(3.24):

$$G = \begin{vmatrix} G_{xx} & G_{xy} & G_{xz} \\ G_{yx} & G_{yy} & G_{yz} \\ G_{zx} & G_{zy} & G_{zz} \end{vmatrix} \quad (3.24)$$

Using equation (3.22) we can define the gravity gradient tensor components in  $k_x, k_y$  plane with the help of the inverse Fourier transform method. If  $\Gamma_{ij}$  refers the gravity gradient tensor in  $k_x, k_y$  then

$$\Gamma_{ij} = \mathcal{F}^{-1}\{[K(\mathbf{k})]G_z(\mathbf{k})\} \quad (3.25)$$

$\therefore$

$$[K(\mathbf{k})] = \begin{pmatrix} \frac{-k_x^2}{|\mathbf{k}|} & \frac{-k_x k_y}{|\mathbf{k}|} & -ik_x \\ \frac{-k_x k_y}{|\mathbf{k}|} & \frac{-k_y^2}{|\mathbf{k}|} & -ik_y \\ -ik_y & -ik_y & |\mathbf{k}| \end{pmatrix} \quad (3.26)$$

where  $|\mathbf{k}| \neq 0, i, j = x, y, z$  and  $\mathcal{F}^{-1}$  represent the operation of inverse Fourier transform. Using this model we have received the entire gradient tensor. Equation (3.25) represents the Inverse FFT of multiplication of the matrix of wave vector with Fourier transform of gravity along  $z$ – direction.

### 3.4 Inverse Model

In recent years, there has been a growing interest in creating precise analytical methods to calculate the mass and spatial location of a moving item using measurements of the gravitational field and gravity gradient tensor(GGT). The inverse model is a novel technique for object detection, the object may be on the surface of the land, submerged in water, or in the air, such as missiles, submersible vehicles, or airplanes. This model requires Gravity Gradient tensor components and gravitational anomaly components to calculate the mass and location of the sub-surface object. The formulas are derived using the forward model [51].

$$x_c = x - \frac{2g_x}{T_{xx} + T_{yy} - \sqrt{(T_{xx} - T_{yy})^2 + 4T_{xy}^2}} \quad (3.27)$$

$$y_c = y - \frac{2g_y}{T_{xx} + T_{yy} - \sqrt{(T_{xx} - T_{yy})^2 + 4T_{xy}^2}} \quad (3.28)$$

$$z_c = z - \frac{2g_z}{T_{xx} + T_{yy} - \sqrt{(T_{xx} - T_{yy})^2 + 4T_{xy}^2}} \quad (3.29)$$

$$M = \frac{4(g_x^2 + g_y^2 + g_z^2)^{\frac{3}{2}}}{T_{xx} + T_{yy} - \sqrt{(T_{xx} - T_{yy})^2 + 4T_{xy}^2}} \quad (3.30)$$

### 3.5 Summary

Using all these models apply numerically to calculate the gravitational acceleration, gravity gradient tensor, mass, and location of the object. The detailed result discuss in the next chapter.

# Chapter 4

## Result and Discussion

### 4.1 Forward Model Calculation

In our model, consider a test mass placed below the observing plane. Assumed the mass is rectangular prismatic with uniform density  $1400\text{kg}/\text{m}^3$ . The height ( $h = 0.5\text{m}$ ) of the body along  $z$ -direction, length ( $l = 1.2\text{m}$ ) along  $y$ -direction and breadth ( $b = 0.9\text{m}$ ) in the  $x$ -direction as shown in Figure 4.1. The mass has been estimated theoretically (A.1) to be  $753\text{kg}$ . The distance  $(\text{PO})=1\text{m}$  between the observing plane to assumed mass. Due to the mass numerically computed the vertical gravity anomaly in **mGal** unit at that point using equation 3.5 which shown in Figure 4.2.

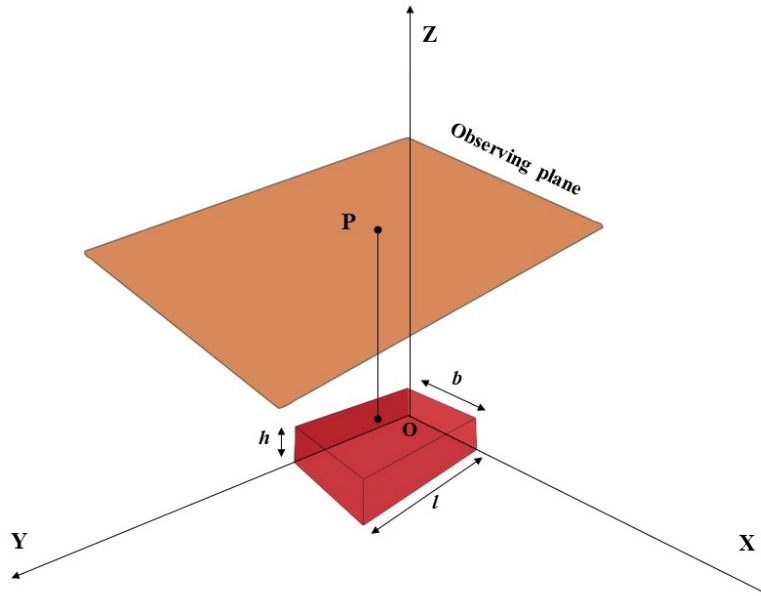


Figure 4.1: Layout of the scheme: Consider a Test prismatic body placed below the surface. we illustrate the variation of gravity anomaly due to this test mass.

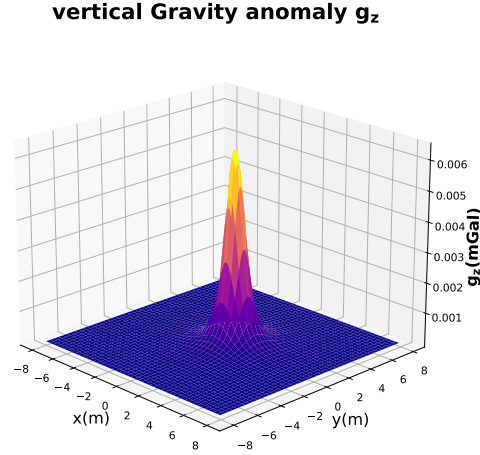
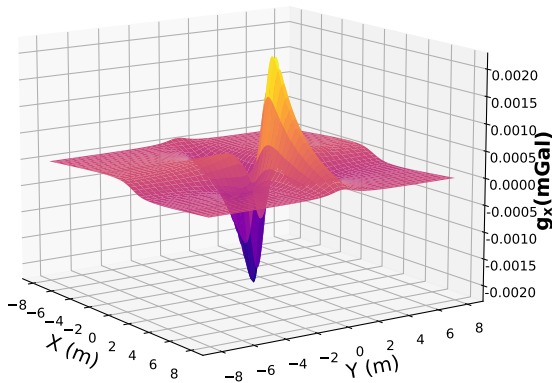


Figure 4.2: Estimated vertical anomaly( $g_z$ )from Forward rectangular prism model in  $mGal$  unit

## 4.2 Compute Horizontal gravity anomaly elements using the Fourier transform technique

Typically, the gravity anomaly varies due to space coordinates acquired using the Forward model discussed in 3.2.1. The benefit of using the Fourier model, we identify the gravity signal along the horizontal direction from the vertical gravity signal. Here numerically interpreted the other two vector components of gravitational acceleration in  $mGal$  using the Fourier model from equation 3.21 which is shown in Figure 4.3.

**Horizontal Gravity anomaly  $g_x$**



**Horizontal Gravity anomaly  $g_y$**

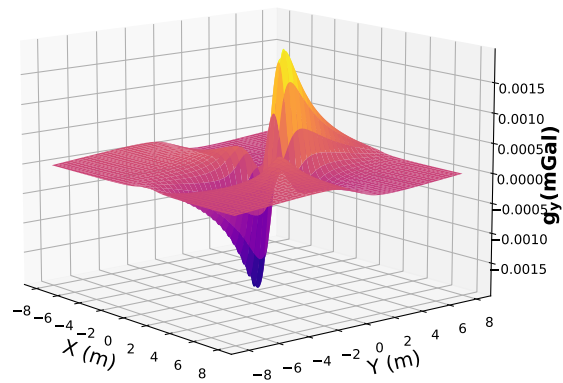
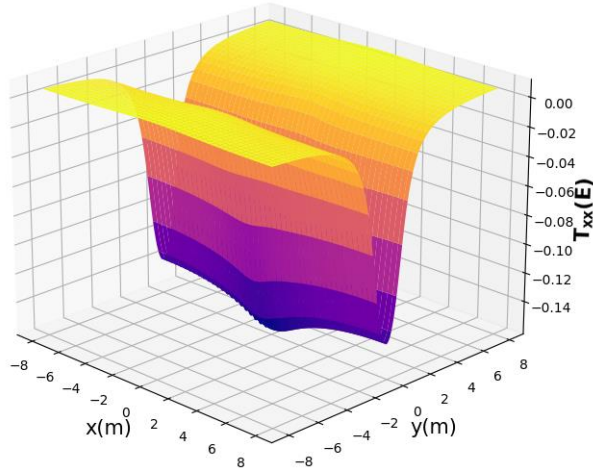


Figure 4.3: Estimation  $g_x$  and  $g_y$  from Fourier Model using vertical gravity anomaly  $g_z$

### 4.3 Nine gravity gradient tensor components demonstrate using the Fourier model

**Gravity Gradient Component  $T_{xx}$**



**Gravity Gradient Component  $T_{xy}$**

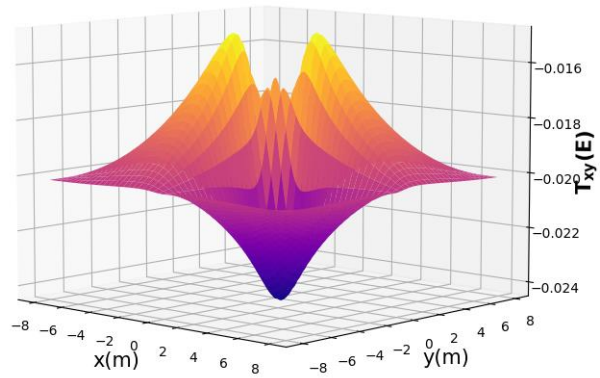
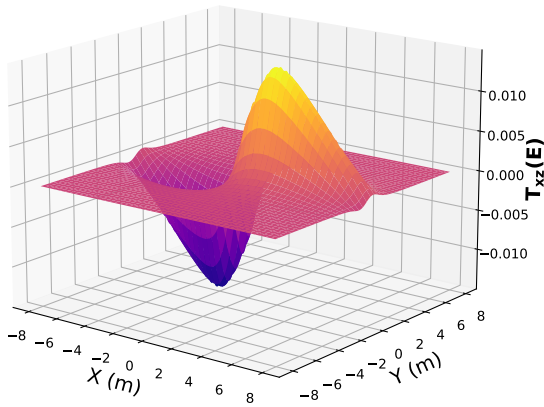


Figure 4.4: Computed of  $T_{xx}$  and  $T_{xy}$  from Fourier Model using vertical gravity anomaly  $g_z$

**Gravity Gradient Component  $T_{xz}$**



**Gravity Gradient Component  $T_{yx}$**

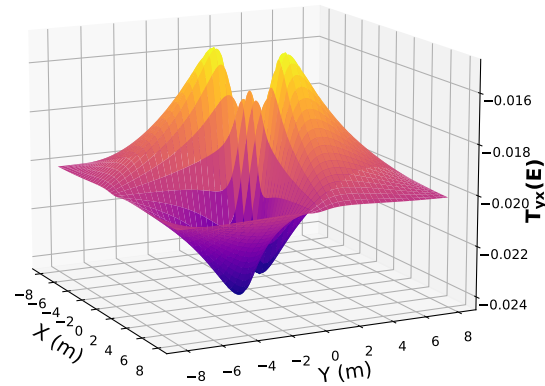


Figure 4.5: FFT derived the  $T_{xz}$  and  $T_{yx}$  components using vertical gravity anomaly  $g_z$

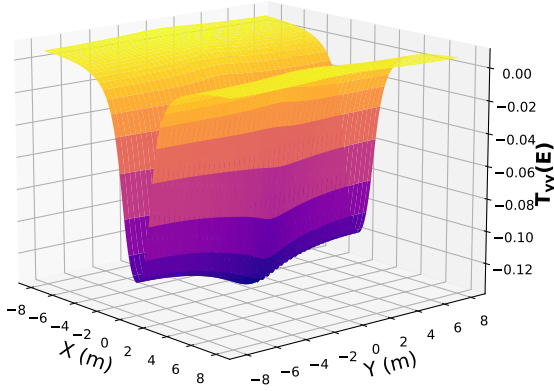
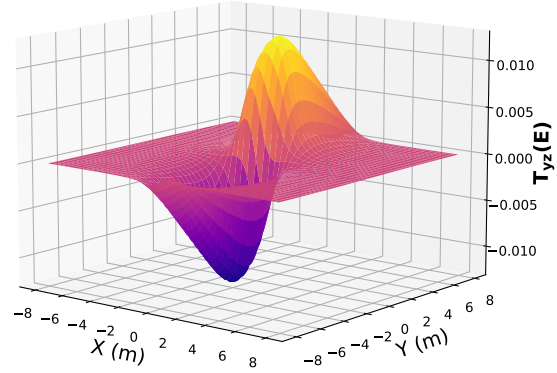
**Gravity Gradient Component  $T_{yy}$** **Gravity Gradient Component  $T_{yz}$** 

Figure 4.6: Evaluated of  $T_{yy}$  and  $T_{yz}$  from Fourier Model with the help of vertical gravity anomaly  $g_z$

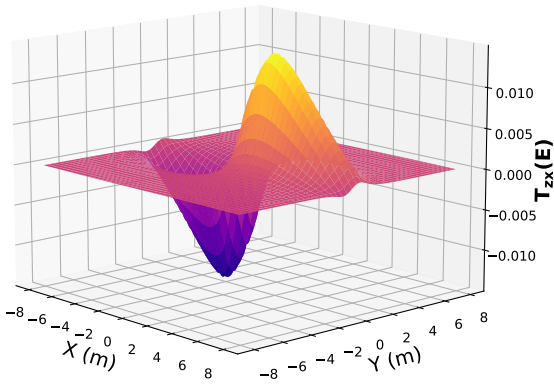
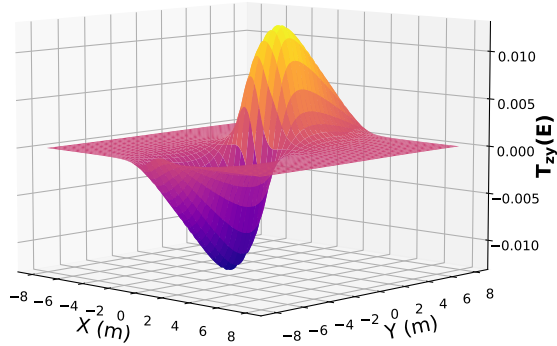
**Gravity Gradient Component  $T_{zx}$** **Gravity Gradient Component  $T_{zy}$** 

Figure 4.7: Computation of  $T_{zx}$  and  $T_{zy}$  from Fourier Model using  $g_z$

Similarly, we can obtain the nine gradient components by using the Forward model (3.2.1). Gradient indicates the spatial change of gravitational signal. These are responsible for the identification of every corner of any object. The forward model can determine the gravity signal for the large masses. It cannot predict the small mass. One of the most reasonable ways is the Fourier transform scheme for point mass detection. Here, we computed computationally all the nine fragments of gravity tensor equations (3.22, 3.25) in eotvos (E) unit shown in this section 4.3

### Gravity Gradient Component $T_{zz}$

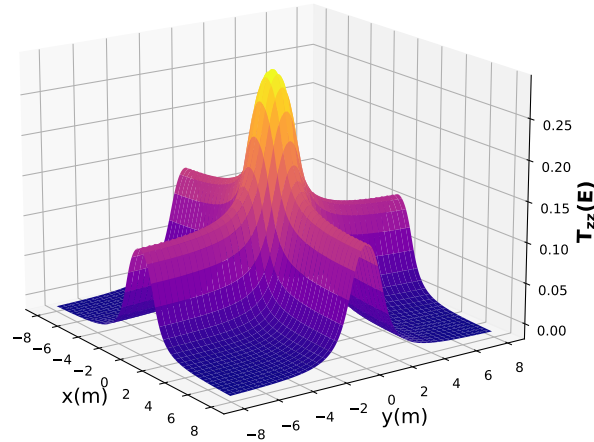


Figure 4.8: Enumeration of  $T_{zz}$  from Fourier Model with use of vertical gravity anomaly  $g_z$

## 4.4 Expected Mass and location of the anomaly

Our goal is point mass detection using a one-dimensional cold atom gravimeter. The inverse model(3.4) technique is the most applicable technique for any type of mass detection. Here, Using equation (3.30) evaluate the expected mass of the body. Figure 4.9 Shows the distribution of the mass of the anomaly. At the height of  $1m$  detected value of the mass is 331Kg. From this plot estimate the center of mass coordinates  $(x,y)$  is  $(0.70,0.52)$ .

This approach can be used to numerically estimate the mass at different depths for distinct objects with variable densities. 4.1 Tabular form of an estimated expected mass of different density rocks and materials. Figure 4.10 shows the linear interpretation of mass with various densities. Table 4.1 tabular form of an estimated expected mass of different density rocks and materials at different depths.

Table 4.1: Variation of mass with density

Object name	Depth (kg/m <sup>3</sup> )	Expected Mass(kg)				
		Depth:10m	Depth:20m	Depth: 30m	Depth: 40m	Depth: 50m
Gold	19300	20.19641	6.286	2.9796	1.7174	1.1116
Silver	10800	11.30161	3.51796	1.6673	0.96104	0.6220
Mild Steel	7850	8.21460	2.5570	1.2119	0.6985	0.4521
Diamond	3520	3.68349	1.1465	0.5434	0.3132	0.2027
Basalt	2850	2.98237	0.9283	0.4399	0.2536	0.1641
Marble	2650	2.77308	0.8632	0.40912	0.2358	0.1526
Granite	2450	2.56379	0.7980	0.37824	0.218014	0.1411
Ballast	1720	1.79988	0.5602	0.26554	0.15305	0.09907



Mass of the anomaly at depth of 1 m

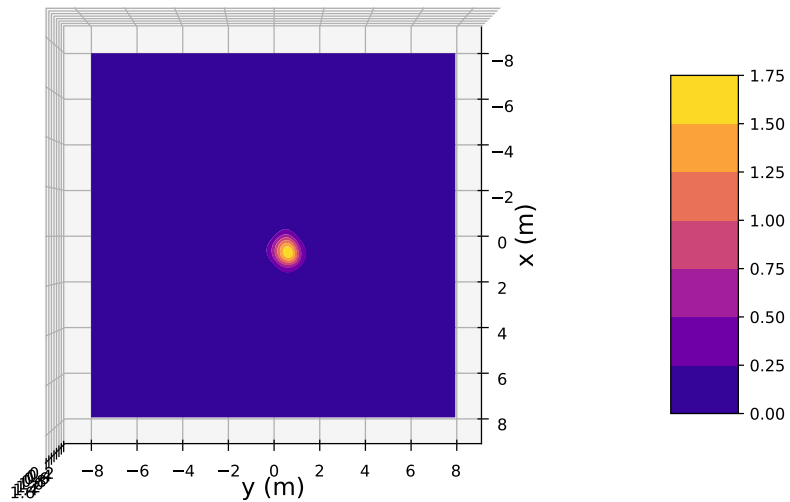
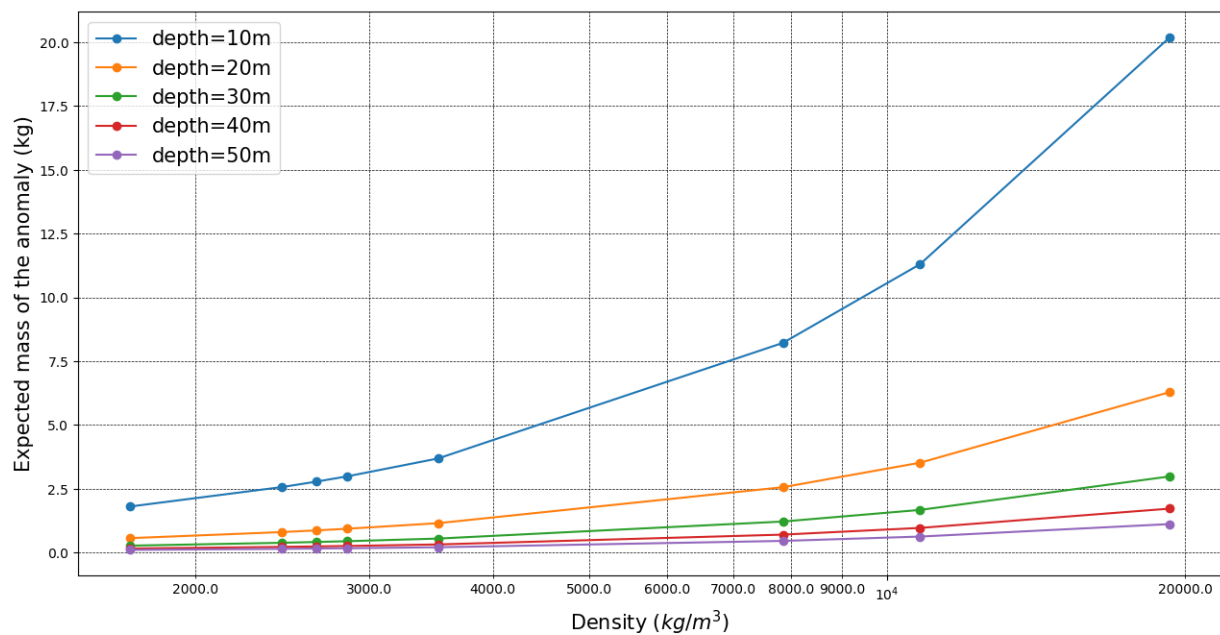


Figure 4.9: Detected Mass of the Anomaly of 331 Kg with an estimated center of Mass coordinate is (from the plot) at (x, y) (0.7000, 0.5260)

Figure 4.10: Estimated mass of the object for different densities



## Chapter 5

# Conclusion and Outlook

A brief history of gravity to atom interferometry was followed by a discussion of the basic principles. It has been discussed how optical molasses and MOT can be used to cool and trap atoms. It is explained how a laser-based atom interferometer of the Mach Zehnder type operates. Since cold atoms are neutral, interact less with the environment's fields, and can have their state altered using laser beams, which is the most important factor for an instrument's precision and sensitivity, we utilize them instead of light. A review of the gravimeters, which are mostly employed for geophysical surveys, and a comparison with the absolute quantum gravimeter follow. Based on the findings and debates made in the current work, this study has created a working understanding. The illustration of how ongoing gravity measurements might improve geophysical monitoring was the main objective of the entire project. Gravity signal readings alter as a result of subsurface mass shifts. The uneven mass distribution within the earth's surface causes variations or changes in gravitational acceleration, which are measured by gravimeters. The earth's observations, archaeological research, and evaluations of subsurface infrastructure can all be done with gravimeters. Deep underground water and gas pipes are used for seismic activity monitoring, oil and mineral exploration mapping, and other purposes. The most popular gravimeter for all of these purposes is an atom interferometer-based quantum gravimeter, which is very accurate, sensitive, and responsive to surrounding noise and vibrations. With the roles of photons and atoms switched, an atom interferometer uses the wave nature of atoms and is similar to an optical Mach Zehnder interferometer. Each element's principle, instrument design, function, history of gravity, gravity anomaly, tensor, and gravity potential were thoroughly explored in this thesis. Further discussed the working principle and comparison of some kind of gravimeter. After that, we focused on some models which help to obtain the gravity anomaly, mass, tensor, etc. This study helps to determine the whole tensor components of gravity, gravitational acceleration, and mass with location.

The model detects point masses and the location of the unknown object with extreme precision which helps in the navigation system. Our scheme is numerically stable. One of the gravimeter's most crucial uses is to locate any underground object utilizing gravity anomaly detection, which we have described in extensive detail. To do this, get the gravity gradient tensor values and signals created by pointlike objects, and then locate the object using the GGT inversion method. We believe that if this technique is used in real

applications we get more accurate results for precise mass detection and gravity signals.

# Appendix A

## A.1 Estimation of Theoretical Mass

Here calculated our theoretical mass of the anomaly. Mass is defined as the multiplication of density and volume. Here we assumed the length( $l$ ), bredth( $b$ ) and height( $h$ ) in meter unit. The volume( $V$ ) is  $0.54m^3$ .

- Size of the anomaly  
 $l : 1.2m$   
 $b : 0.9m$   
 $h : 0.5m$
- Volume ( $V$ ) =  $l \times b \times h = 0.54m^3$
- Density of the anomaly ( $\rho$ ) =  $1400kg/m^3$
- **Mass**=  $\rho \times V = 1400 * 0.54 = 756kg$

# Bibliography

- [1] Benjamin P Abbott, Richard Abbott, TD Abbott, MR Abernathy, Fausto Acernese, Kendall Ackley, Carl Adams, Thomas Adams, Paolo Addesso, RX Adhikari, et al. Observation of gravitational waves from a binary black hole merger. *Physical review letters*, 116(6):061102, 2016.
- [2] Terry Quinn. Measuring big g. *Nature*, 408(6815):919–920, 2000.
- [3] George T Gillies. The newtonian gravitational constant: recent measurements and related studies. *Reports on Progress in Physics*, 60(2):151, 1997.
- [4] John Archibald Wheeler Ignazio Ciufolini. *Gravitation and Inertia*. Princeton University Press, 1995.
- [5] Wolfgang Torge. Gravity and height variations connected with the current rifting episode in northern iceland. *Tectonophysics*, 71(1-4):227–240, 1981.
- [6] R Rummel. Geoid and gravity in earth sciences—an overview. *Future Satellite Gravimetry and Earth Dynamics*, pages 3–11, 2005.
- [7] Iginio Marson. A short walk along the gravimeters path. *International Journal of Geophysics*, 2012, 2012.
- [8] A Wicht, JM Hensley, E Sarajlic, and S Chu. Precision measurement of the fine structure constant based on atom interferometry. In *2003 European Quantum Electronics Conference. EQEC 2003 (IEEE Cat No. 03TH8665)*, page 272. IEEE, 2003.
- [9] J. Hinderer, D. Crossley, and R. J. Warburton. Gravimetric Methods - Superconducting Gravity Meters. In Gerald Schubert, editor, *Planets and Moons*, volume 10, pages 65–122. 2007.
- [10] Shuhei Okubo, Shigeo Yoshida, Tadahiro Sato, Yoshiaki Tamura, and Yuichi Imanishi. Verifying the precision of a new generation absolute gravimeter FG5—Comparison with superconducting gravimeters and detection of oceanic load-ing tide. , 24(4):489–492, February 1997.
- [11] Umberto Riccardi, Severine Rosat, and Jacques Hinderer. On the accuracy of the cali-bration of superconducting gravimeters using absolute and spring sensors: a critical comparison. *Pure and Applied Geophysics*, 169:1343–1356, 2012.

- [12] R Reudink, R Klees, Olivier Francis, J Kusche, R Schlesinger, Akbar Shabanloui, N Sneeuw, and L Timmen. High tilt susceptibility of the scintrex cg-5 relative gravimeters. *Journal of Geodesy*, 88:617–622, 2014.
- [13] Andrzej Kotyrba and Lukasz Kortas. Co-seismic signals of mining tremors in continuous recordings of gravity by gphonex tidal gravimeters. *International Journal of Rock Mechanics and Mining Sciences*, 129:104288, 2020.
- [14] Jacques Hinderer, D Crossley, and RJ Warburton. Gravimetric methods-superconducting gravity meters. *Planets and Moons. Treatise on Geophysics*, 10:65–122, 2007.
- [15] RP Middlemiss, Antonio Samarelli, DJ Paul, James Hough, Sheila Rowan, and GD Hammond. Measurement of the earth tides with a mems gravimeter. *Nature*, 531(7596):614–617, 2016.
- [16] Alena Pešková and Martin Štroner. Adjustment and testing comparison of absolute gravimeters in november 2013. *Geoinformatics FCE CTU*, 16(1):79–90, 2017.
- [17] M Van Camp, Th Camelbeeck, and P Richard. The fg5 absolute gravimeter: metrology and geophysics. *Physica Magazine, Journal of the Belgian Society*, 25(3):161–174, 2003.
- [18] ALESSANDRO Germak, S Desogus, and C Origlia. Interferometer for the imgc rise-and-fall absolute gravimeter. *Metrologia*, 39(5):471, 2002.
- [19] TM Niebauer, GS Sasagawa, James E Faller, R Hilt, and Fred Klopping. A new generation of absolute gravimeters. *Metrologia*, 32(3):159, 1995.
- [20] Lingxiao Zhu, Yu-Hung Lien, Andrew Hinton, Alexander Niggebaum, Clemens Rammeloo, Kai Bongs, and Michael Holynski. Application of optical single-sideband laser in raman atom interferometry. *Optics express*, 26(6):6542–6553, 2018.
- [21] Mark Kasevich and Steven Chu. Measurement of the gravitational acceleration of an atom with a light-pulse atom interferometer. *Applied Physics B*, 54:321–332, 1992.
- [22] G Lamporesi, A Bertoldi, L Cacciapuoti, Marco Prevedelli, and Guglielmo M Tino. Determination of the newtonian gravitational constant using atom interferometry. *Physical Review Letters*, 100(5):050801, 2008.
- [23] K Pant, P Arora, S Yadav, and A Sengupta. Generation of quadrupole magnetic field for trapping atoms in cs fountain being developed at npl india. *Mapan*, 26(4):285–294, 2011.
- [24] Maurizio Battaglia, Joachim Gottsmann, Daniele Carbone, and José Fernández. 4d volcano gravimetry. *Geophysics*, 73(6):WA3–WA18, 2008.

- [25] Ben Stray, Andrew Lamb, Aisha Kaushik, Jamie Vovrosh, Anthony Rodgers, Jonathan Winch, Farzad Hayati, Daniel Boddice, Artur Stabrawa, Alexander Niggelbaum, et al. Quantum sensing for gravity cartography. *Nature*, 602(7898):590–594, 2022.
- [26] Tim Kovachy, Peter Asenbaum, Chris Overstreet, Christine A Donnelly, Susannah M Dickerson, Alex Sugarbaker, Jason M Hogan, and Mark A Kasevich. Quantum superposition at the half-metre scale. *Nature*, 528(7583):530–533, 2015.
- [27] Sheng-wei Chiow, Tim Kovachy, Hui-Chun Chien, and Mark A Kasevich. 102 k large area atom interferometers. *Physical review letters*, 107(13):130403, 2011.
- [28] Renée Charrière, Malo Cadoret, Nassim Zahzam, Yannick Bidet, and Alexandre Bresson. Local gravity measurement with the combination of atom interferometry and bloch oscillations. *Physical Review A*, 85(1):013639, 2012.
- [29] Jason Williams, Sheng-wei Chiow, Nan Yu, and Holger Müller. Quantum test of the equivalence principle and space-time aboard the international space station. *New Journal of Physics*, 18(2):025018, 2016.
- [30] P Berg, S Abend, G Tackmann, Ch Schubert, Enno Giese, Wolfgang P Schleich, FA Narducci, W Ertmer, and EM Rasel. Composite-light-pulse technique for high-precision atom interferometry. *Physical review letters*, 114(6):063002, 2015.
- [31] MJ Snadden, JM McGuirk, P Bouyer, KG Haritos, and MA Kasevich. Measurement of the earth’s gravity gradient with an atom interferometer-based gravity gradiometer. *Physical review letters*, 81(5):971, 1998.
- [32] B Barrett, A Bertoldi, and P Bouyer. Inertial quantum sensors using light and matter. *Physica Scripta*, 91(5):053006, 2016.
- [33] P Cheinet, F Pereira Dos Santos, T Petelski, A Clairon, N Dimarcq, D Holleville, and A Landragin. Cold atom absolute gravimeter for the watt balance. In *2004 Conference on Precision Electromagnetic Measurements*, pages 60–61. IEEE, 2004.
- [34] A Bertoldi, G Lamporesi, L Cacciapuoti, M De Angelis, M Fattori, T Petelski, A Peters, M Prevedelli, J Stuhler, and GM Tino. Atom interferometry gravity-gradiometer for the determination of the newtonian gravitational constant  $g$ . *The European Physical Journal D-Atomic, Molecular, Optical and Plasma Physics*, 40:271–279, 2006.
- [35] Lin Zhou, Shitong Long, Biao Tang, Xi Chen, Fen Gao, Wencui Peng, Weitao Duan, Jiaqi Zhong, Zongyuan Xiong, Jin Wang, et al. Test of equivalence principle at  $10^{-8}$  level by a dual-species double-diffraction raman atom interferometer. *Physical review letters*, 115(1):013004, 2015.
- [36] Jason M Hogan, David MS Johnson, Susannah Dickerson, Tim Kovachy, Alex Sugarbaker, Sheng-wei Chiow, Peter W Graham, Mark A Kasevich, Babak Saif, Surjeet Rajendran, et al. An atomic gravitational wave interferometric sensor in low earth orbit (agis-leo). *General Relativity and Gravitation*, 43:1953–2009, 2011.

- [37] Paul Hamilton, Matt Jaffe, Philipp Haslinger, Quinn Simmons, Holger Müller, and Justin Khoury. Atom-interferometry constraints on dark energy. *Science*, 349(6250):849–851, 2015.
- [38] GL Gattobigio, T Pohl, G Labeyrie, and R Kaiser. Scaling laws for large magneto-optical traps. *Physica Scripta*, 81(2):025301, 2010.
- [39] Paul D Lett, Richard N Watts, Christoph I Westbrook, William D Phillips, Phillip L Gould, and Harold J Metcalf. Observation of atoms laser cooled below the doppler limit. *Physical review letters*, 61(2):169, 1988.
- [40] AM Steane, M Chowdhury, and CJ Foot. Radiation force in the magneto-optical trap. *JOSA B*, 9(12):2142–2158, 1992.
- [41] DP Dai, Y Xia, YN Yin, XX Yang, YF Fang, XJ Li, and JP Yin. A linewidth-narrowed and frequency-stabilized dye laser for application in laser cooling of molecules. *Optics Express*, 22(23):28645–28652, 2014.
- [42] DS Goodman, I Sivarajah, JE Wells, FA Narducci, and WW Smith. Ion–neutral-atom sympathetic cooling in a hybrid linear rf paul and magneto-optical trap. *Physical Review A*, 86(3):033408, 2012.
- [43] Daniel A Steck. Quantum and atom optics. 2007.
- [44] Daniel A Steck. Rubidium 87 d line data, 2001. URL <http://steck.us/alkalidata>, 83:13, 2016.
- [45] Harold J Metcalf and Peter van der Straten. Laser cooling and trapping of atoms. *JOSA B*, 20(5):887–908, 2003.
- [46] Isidor Isaac Rabi, Sidney Millman, Polykarp Kusch, and Jerrold Reinach Zacharias. The molecular beam resonance method for measuring nuclear magnetic moments. the magnetic moments of li 6 3, li 7 3 and f 19 9. *Physical review*, 55(6):526, 1939.
- [47] Alexander Niggebaum. *Towards mobile quantum sensors for gravity surveys*. PhD thesis, University of Birmingham, 2016.
- [48] Donald Plouff. Derivation of formulas and fortran programs to compute gravity anomalies of prisms. *Final Report*, 1975.
- [49] Donald Plouff. Gravity and magnetic fields of polygonal prisms and application to magnetic terrain corrections. *Geophysics*, 41(4):727–741, 1976.
- [50] Kevin L Mickus and Juan Homero Hinojosa. The complete gravity gradient tensor derived from the vertical component of gravity: a fourier transform technique. *Journal of Applied Geophysics*, 46(3):159–174, 2001.



- [51] Jingtian Tang, Shuanggui Hu, Zhengyong Ren, Chaojian Chen, Xiao Xiao, and Cong Zhou. Analytical formulas for underwater and aerial object localization by gravitational field and gravitational gradient tensor. *IEEE Geoscience and Remote Sensing Letters*, 14(9):1557–1560, 2017.
- [52] Xiong Li and Michel Chouteau. Three-dimensional gravity modeling in all space. *Surveys in Geophysics*, 19(4):339–368, 1998.
- [53] Rene Forsberg. A study of terrain reductions, density anomalies and geophysical inversion methods in gravity field modelling. 1984.
- [54] Richard J Blakely. *Potential theory in gravity and magnetic applications*. Cambridge university press, 1996.